Article:
Khare, Shilpi, Nagle, Advait S, Biggart, Agnes et al. (2016) Proteasome inhibition for treatment of leishmaniasis, Chagas disease and sleeping sickness. Nature. pp. 229-233. ISSN: 0028-0836

https://doi.org/10.1038/nature19339

Proteasome inhibition for treatment of leishmaniasis, Chagas disease and sleeping sickness

Shilpi Khare[1*], Advait S. Nagle[1*], Agnes Biggart[1], Yin H. Lai[1], Fang Liang[1], Lauren C. Davis[1], S. Whitney Barnes[1], Casey J. N. Mathison[1], Elmarie Myburgh[2,3], Mu-Yun Gao[1], J. Robert Gillespie[4], Xianzhong Liu[1], Jocelyn L. Tan[1], Monique Stinson[1], Ianne C. Rivera[1], Jaime Ballard[1], Vince Yeh[1], Todd Groessl[1], Glenn Federe[1], Hazel X. Y. Koh[5], John D. Venable[1], Badry Bursulaya[1], Michael Shapiro[1], Pranab K. Mishra[1], Glen Spraggon[1], Ansgar Brock[1], Jeremy C. Mottram[2,3], Frederick S. Buckner[4], Srinivasa P. S. Rao[5], Ben G. Wen[1], John R. Walker[1], Tove Tuntland[1], Valentina Molteni[1], Richard J. Glynne[1] & Frantisek Supek[1]

Chagas disease, leishmaniasis, and sleeping sickness affect 20 million people worldwide and lead to more than 50,000 deaths annually[1]. The diseases are caused by infection with the kinetoplastid parasites *Trypanosoma cruzi, Leishmania* spp. and *Trypanosoma brucei* spp., respectively. These parasites have similar biology and genomic sequence, suggesting that all three diseases could be cured with drug(s) modulating the activity of a conserved parasite target[2]. However, no such molecular targets or broad spectrum drugs have been identified to date. Here we describe a selective inhibitor of the kinetoplastid proteasome (GNF6702) with unprecedented *in vivo* efficacy, which cleared parasites from mice in all three models of infection. GNF6702 inhibits the kinetoplastid proteasome through a non-competitive mechanism, does not inhibit the mammalian proteasome or growth of mammalian cells, and is well-tolerated in mice. Our data provide genetic and chemical validation of the parasite proteasome as a promising therapeutic target for treatment of kinetoplastid infections, and underscore the possibility of developing a single class of drugs for these neglected diseases.

Kinetoplastid infections affect predominantly poor communities in Latin America, Asia and Africa. Available therapies suffer from multiple shortcomings, and new drug discovery for these diseases is limited by insufficient investment[3]. We sought low molecular weight compounds with a growth inhibitory effect on *Leishmania donovani* (*L. donovani*)[4,5], *Trypanosoma cruzi* (*T. cruzi*)[6,7] and *Trypanosoma brucei* (*T. brucei*)[5,8]. Our approach was to test 3 million compounds in proliferation assays on all three parasites (Supplementary Information Tables 1-3), followed by triaging of active compounds (half-maximum inhibitory concentration value EC_{50}<10 μM) to select those with a clear window of selectivity (>5-fold) with respect to growth inhibition of mammalian cells. An azabenzoxazole, GNF5343, was identified as a hit in the *L. donovani* and *T. brucei* screens. Although GNF5343 was not identified in the *T. cruzi* screen, we noted potent anti-*T. cruzi* activity of this compound in secondary assays.

Optimization of GNF5343 involved the design and synthesis of ~3,000 compounds, and focused on improving bioavailability and potency on inhibition of *L. donovani* growth within macrophages (Fig. 1). A critical modification involved replacement of the azabenzoxazole center with C6-substituted imidazo- and triazolopyrimidine cores, which yielded compounds up to 20-fold more potent on intra-macrophage *L. donovani* (e.g. GNF2636). Replacement of the furan group with a dimethyloxazole ring reduced the risk of toxicity associated with the furan moiety, and replacement of the chlorophenyl group with a fluorophenyl improved selectivity over mammalian cell growth inhibition (e.g. GNF3849). These changes also resulted in low clearance and acceptable bioavailability. Further substitutions at the core C6 position led to GNF6702 and a 400-fold increase in intra-macrophage *L. donovani* potency compared to GNF5343.

L. donovani parasites cause a majority of visceral leishmaniasis (VL) cases in East Africa and India[9]. In mice infected with *L. donovani*[10], oral dosing with GNF6702 effected a more pronounced reduction in

liver parasite burden than miltefosine, the only oral anti-leishmanial drug available in clinical practice[5] (Fig. 2a). The miltefosine regimen for VL efficacy studies was chosen to approximate the drug plasma concentration of the clinical regimen[11]. We noted a greater than three log reduction in parasite load after eight day treatment with 10 mg/kg of GNF6702 twice-daily with the free concentration of GNF6702 (fraction unbound in plasma=0.063) staying above the *L. donovani* EC_{99} value (the concentration inhibiting 99% of intra-macrophage parasite growth *in vitro*) for the duration of the dosing period (Extended Data Fig. 1a). Characterization of efficacy of ten analogues in the series at various doses revealed a significant correlation (r^2=0.89, $p<0.01$) between i) the ratio of mean free plasma compound concentration to the *L. donovani* EC_{90} value and ii) reduction of the liver parasite burden. We found that 90% parasite burden reduction in the mouse model was achieved when the mean free compound plasma concentration during treatment equaled a 0.94-fold multiple of the *L. donovani* EC_{90} value (Fig. 2b).

Cutaneous leishmaniasis (CL) affects about a million people per year, causing skin lesions that can resolve into scar tissue[12]. In parts of the Middle East, CL has reached epidemic proportions[13]. After footpad infection of BALB/c mice with the dermatotropic *L. major* strain[14,15], treatment with GNF6702 at 10 mg/kg twice-daily caused a 5-fold decrease in footpad parasite burden and a reduction in footpad swelling (Fig. 2c). Both 3 mg/kg and 10 mg/kg twice-daily regimens of GNF6702 were superior to 30 mg/kg once-daily miltefosine regimen ($p<0.01$), which translates into ~2-fold higher miltefosine plasma concentration in mice than observed in clinical dosing[11].

We further tested if GNF6702 can cure additional kinetoplastid parasite infections. An estimated 25% of the 8 million people infected with *T. cruzi* will develop chronic Chagas disease, manifesting as cardiac or intestinal dysfunction[16,17]. Benznidazole is broadly used for treatment of acute and indeterminate stages of Chagas disease in Latin America[18,19]. However, benznidazole has side-effects that frequently lead to treatment interruption[18,20-22] and a better tolerated drug is needed. To model treatment in the

indeterminate disease stage, we infected mice with *T. cruzi* parasites and began treatment 35 days after infection, when the immune system of the mice had controlled parasite burden[23]. We increased the parasite detection sensitivity by immunosuppressing the mice after 20 days of treatment[23,24]. In this model, GNF6702 dosed twice-daily at 10 mg/kg matched the efficacy of benznidazole at 100 mg/kg once-daily; all but one treated mice had no detectable parasites in blood, colon or heart tissue, even after 4 weeks of immunosuppression (Fig. 2d).

Finally, we tested GNF6702 in a mouse model of stage II sleeping sickness (human African trypanosomiasis - HAT)[25]. Mortality of stage II HAT is caused by infection of the CNS and, in this mouse model, luciferase-expressing *T. brucei* parasites establish a CNS infection by day 21 post-infection. GNF6702 was administered at 100 mg/kg once-daily to account for low exposure in the brain relative to the plasma (~10%, Extended Data Fig. 1b). Diminazene aceturate, a stage I drug that poorly crosses the blood-brain barrier, effected apparent clearance of parasites from the blood after a single dose, but did not prevent parasite recrudescence 21 days later. By contrast, treatment with GNF6702 for seven days caused a sustained clearance of parasites (days 42 and 92 post-infection in Fig. 2e, Extended Data Fig. 2a, Supplementary Information Tables 4 and 5). Significantly, mice treated with GNF6702 had no detectable parasites in the brain at termination of the experiment, though parasites were clearly detected in the brains of mice treated with diminazene aceturate (Extended Data Fig. 2b, Supplementary Information Table 6).

As GNF6702 showed compelling efficacy in four mouse models of kinetoplastid infections: VL, CL, Chagas disease and stage II HAT, we reasoned that mechanistic studies of GNF6702 might identify a pan-kinetoplastid drug target that could inform target-based drug discovery efforts. We attempted to evolve *L. donovani* strains resistant to GNF3943 and GNF8000 (early analogues from the series, Extended Data Fig. 3) through 12 months of parasite culture under drug pressure without success.

However, we were able to select two drug-resistant *T. cruzi* epimastigote isolates, one resistant to GNF3943, and another to GNF8000. Both *T. cruzi* lines exhibited at least 40-fold lower susceptibility to GNF6702 than wild type *T. cruzi* (Extended Data Fig. 4a and 4b). Using whole genome sequencing, we found that the GNF3943-resistant line had a homozygous mutation encoding a substitution of isoleucine for methionine at amino acid 29 in the proteasome beta 4 subunit ($PSMB4^{I29M/I29M}$) and a heterozygous mutation P82L in dynein heavy chain gene. The GNF8000-resistant line had a heterozygous F24L mutation in *PSMB4,* and four other heterozygous mutations (Extended Data Table 1). We focused our attention on the proteasome as a likely target for the compound series because we found two independent mutations in the *PSMB4* gene, and because the proteasome is an essential enzyme in eukaryotic cells. We also note that the *Plasmodium falciparum* proteasome has recently been the target of promising drug discovery efforts for malaria[26].

We first asked whether two prototypic inhibitors of mammalian proteasome, bortezomib and MG132, could also block *T. cruzi* growth. Indeed, both compounds inhibited *T. cruzi* epimastigote proliferation with sub-micromolar potency. However, in contrast to GNF6702, bortezomib and MG132 inhibited proliferation of the two resistant lines ($PSMB4^{I29M/I29M}$, $PSMB4^{wt/F24L}$) with comparable potency to the wild type parasites. Additionally, the *PSMB4* mutant lines were not resistant to nifurtimox, an anti-kinetoplastid drug with an unrelated mechanism of action (Extended Data Fig. 4a and 4b). To determine whether the F24L mutation was sufficient to confer resistance to GNF6702, we engineered *T. cruzi* epimastigote lines that ectopically expressed either wild type or F24L-mutated PSMB4. Overexpression of $PSMB4^{WT}$ had little effect on the EC_{50} value for GNF6702, whereas overexpression of $PSMB4^{F24L}$ caused a greater than 10-fold reduction in GNF6702 potency, but not in that of bortezomib (Fig. 3a, Extended Data Fig. 4c). Previously, bortezomib was also shown to inhibit the growth of *T. brucei,* suggesting that proteasome activity is essential for growth in this parasite as well[27]. To test whether

PSMB4^{F24L} can rescue growth inhibition by GNF6702 in *T. brucei*, we engineered two parasite strains that ectopically expressed wild type and F24L-mutated PSMB4, respectively. Similar to *T. cruzi*, overexpression of PSMB4^{F24L} in *T. brucei* conferred a high level of resistance to GNF6702 (~70-fold shift in EC_{50} value), while having no effect on parasite susceptibility to bortezomib (Fig. 3b, Extended Data Fig. 4c).

We next asked whether GNF6702 could inhibit any of three *T. cruzi* proteasome proteolytic activities in biochemical assays. As predicted from the *T. cruzi* genome[28], mass spectrometry analysis of purified *T. cruzi* proteasome identified seven alpha and seven beta proteasome subunits, including PSMB4 (Supplementary Tables 7 and 8). Using substrates that are specific for each of the chymotrypsin-like, trypsin-like and caspase-like proteolytic activities, we found that only the chymotrypsin-like activity of the *T. cruzi* proteasome was inhibited by GNF6702 (IC_{50}=35 nM), while the other two activities were not affected (IC_{50}>10 μM). In contrast, bortezomib inhibited the chymotrypsin-like (IC_{50}=91 nM), the caspase-like (IC_{50}=370 nM) and the trypsin-like (IC_{50}=1.7 μM) activities. We further found that the chymotrypsin-like activity of the PSMB4^{I29M} *T. cruzi* proteasome was at least 300-fold less susceptible to GNF6702 (IC_{50}>10 μM) and ~3-fold less susceptible to bortezomib (IC_{50}=0.26 μM), while susceptibility of the other two mutant proteasome proteolytic activities to the two inhibitors were not affected (Fig. 4a, Extended Data Table 2).

We reasoned that if the primary mechanism of parasite growth inhibition by the compound series was through inhibition of the proteasome chymotrypsin-like activity, then the IC_{50} values for this proteolytic activity should correlate with EC_{50} values for parasite proliferation. Indeed, a tight correlation between the two parameters was observed for *L. donovani* axenic amastigotes and *T. brucei* bloodstream form trypomastigotes (r^2=0.78 and r^2=0.67, respectively) over a 2,000-fold potency range for 317 analogues, thus indicating that inhibition of parasite proteasome activity was driving the anti-parasitic activity of

these compounds. We observed a weaker correlation between IC_{50} and EC_{50} values for intracellular *T .cruzi* (r^2=0.36, p<0.01), perhaps reflecting more complex cellular pharmacokinetics resulting from compounds having to access *T. cruzi* parasites within the cytosol of mammalian cells (Fig. 4b, Extended Data Fig. 5).

Both resistant *T. cruzi* lines retained sensitivity to bortezomib, which is a substrate-competitive inhibitor, suggesting that GNF6702 might have an alternative mode of inhibition. A Lineweaver-Burk plot of chymotrypsin-like activity at increasing concentrations of peptide substrate showed that GNF6702 has a non-competitive mode of inhibition clearly distinct from the competitive mechanism described for MG132 and bortezomib[29,30]. We were also able to extend these observations to proteasome from *L. donovani* (Fig. 4c, Extended Data Table 3). We further note that GNF6702 had no measurable activity on the human proteasome (Fig. 4d, Extended Data Table 2). Interestingly, human proteasome beta 4 subunit has a methionine at the 29th amino acid position, mirroring the I29M mutation in the GNF3943-resistant *T. cruzi* line (Extended Data Fig. 6a).

In summary, GNF6702 blocks the chymotrypsin-like activity harbored by the beta 5 subunit without competing with substrate binding, and mutations in the beta 4 subunit, which is in direct physical contact with the beta 5 subunit, confer resistance to this inhibition. Next we used homology modeling of the *T. cruzi* proteasome to look for evidence of an allosteric inhibitor binding site. In the *T. cruzi* proteasome model, the F24 and I29 beta 4 residues are positioned at the interface between the beta 4 and beta 5 subunits, on the outer limit of the beta 5 active site. Adjacent to these two beta 4 residues and the beta 5 active site is a plausible binding pocket for GNF6702 (Extended Data Fig. 6b and 6c).

Finally, we tested whether GNF6702 can inhibit proteasome activity in intact *T. cruzi* cells. Cellular proteins entering the proteasome degradation pathway are first tagged with ubiquitin, and proteasome inhibition results in intracellular accumulation of ubiquitylated proteins. Treatment of *T. cruzi*

161 epimastigotes with GNF6702 led to significant buildup of ubiquitylated proteins (Extended Data Fig. 7a)
162 with the half-maximal effect (EC_{50}) achieved at 130 nM compound concentration (Extended Data Fig.
163 7c). This EC_{50} value correlated well with the half-maximal growth inhibitory concentration of GNF6702
164 on *T. cruzi* epimastigotes (EC_{50}=150 nM; Extended Data Fig. 4b). For comparison, similar experiments
165 with bortezomib yielded comparable inhibitor potencies in the two *T. cruzi* assays (ubiquitylation
166 EC_{50}=62 nM *vs* growth inhibition EC_{50}=160 nM; Extended Data Fig. 4b and 7c). We did not observe any
167 detectable accumulation of ubiquitylated proteins in mammalian 3T3 cells treated with GNF6702
168 (Extended Data Fig. 7b and 7c), further confirming high selectivity of this compound.
169 Validation of the parasite proteasome as the target of GNF6702 is supported through several lines of
170 evidence: i) point mutations in the *PSMB4* gene are sufficient to confer resistance to biochemical
171 proteasome inhibition and cellular *T. cruzi* growth inhibition; ii) GNF6702 is a selective inhibitor of
172 parasite proteasome activity and does not inhibit the human proteasome, mirroring the selective
173 inhibition of parasite growth over mammalian cell growth; and iii) potency of GNF6702 and analogues in
174 parasite proteasome assays predict potency in parasite growth inhibition assays.
175 In this work we show that in mouse disease models, GNF6702 was able to eradicate parasites from
176 diverse niches that included the cytosol (*T. cruzi*), phagolysosome (*L. donovani, L. major*) of infected
177 host cells, and brain (*T. brucei*). GNF6702 has also good pharmacokinetic properties, and the compound
178 did not show activity in panels of human receptor, enzyme and ion channel assays (Supplementary
179 Tables 9-11). Going forward, GNF6702, or analogues thereof, has potential to yield a new treatment for
180 several kinetoplastid infections and it is currently being evaluated in preclinical toxicity studies. It is
181 unclear if the clinical utility of GNF6702 could extend to the treatment of stage II HAT as GNF6702 was
182 tested in the HAT mouse model only at one high dose (100 mg/kg once-daily). We also note that
183 identification of a broadly active pan-kinetoplastid drug might not be feasible (or desirable) as such a

drug would need to reach high concentrations in varied tissues/subcellular compartments, and might carry increased toxicity risk. Instead, alternative analogues from this series with different pharmacological profiles might be needed for treatment of different kinetoplastid infections. Nevertheless, there are only scarce resources for drug development in these diseases, and identification of a common target and chemical scaffold with potential across multiple indications provides new hope for improved treatment options for some of the world's poorest people.

REFERENCES

1. Research priorities for Chagas disease, human African trypanosomiasis and leishmaniasis. *World Health Organization, WHO Technical Report Series* 975, 1-100 (2012).
2. El-Sayed, N. M. *et al.* Comparative genomics of trypanosomatid parasitic protozoa. *Science* 309, 404-409, doi:10.1126/science.1112181 (2005).
3. Bilbe, G. Infectious diseases. Overcoming neglect of kinetoplastid diseases. *Science* 348, 974-976, doi:10.1126/science.aaa3683 (2015).
4. Sundar, S. & Chakravarty, J. An update on pharmacotherapy for leishmaniasis. *Expert Opinion on Pharmacotherapy* 16, 237-252, doi:10.1517/14656566.2015.973850 (2015).
5. Nagle, A. S. *et al.* Recent developments in drug discovery for leishmaniasis and human African trypanosomiasis. *Chemical Reviews*, doi:10.1021/cr500365f (2014).
6. Bern, C. Chagas' Disease. *The New England Journal of Medicine* 373, 456-466, doi:10.1056/NEJMra1410150 (2015).
7. Chatelain, E. Chagas disease drug discovery: toward a new era. *Journal of Biomolecular Screening* 20, 22-35, doi:10.1177/1087057114550585 (2015).

8. Kennedy, P. G. Clinical features, diagnosis, and treatment of human African trypanosomiasis (sleeping sickness). *The Lancet. Neurology* 12, 186-194, doi:10.1016/S1474-4422(12)70296-X (2013).
9. Control of the leishmaniases. *World Health Organization, WHO Technical Report Series* 949, 37-39 (2010).
10. Yardley, V. & Croft, S. L. A comparison of the activities of three amphotericin B lipid formulations against experimental visceral and cutaneous leishmaniasis. *International Journal of Antimicrobial Agents* 13, 243-248 (2000).
11. Dorlo, T. P. *et al.* Pharmacokinetics of miltefosine in Old World cutaneous leishmaniasis patients. *Antimicrobial Agents and Chemotherapy* 52, 2855-2860, doi:10.1128/AAC.00014-08 (2008).
12. McGwire, B. S. & Satoskar, A. R. Leishmaniasis: clinical syndromes and treatment. *QJM : Monthly journal of the Association of Physicians* 107, 7-14, doi:10.1093/qjmed/hct116 (2014).
13. Hotez, P. J. Combating the next lethal epidemic. *Science* 348, 296-297, doi:10.1126/science.348.6232.296-b (2015).
14. Sacks, D. & Anderson, C. Re-examination of the immunosuppressive mechanisms mediating non-cure of *Leishmania* infection in mice. *Immunological Reviews* 201, 225-238, doi:10.1111/j.0105-2896.2004.00185.x (2004).
15. Nelson, K. G., Bishop, J. V., Ryan, R. O. & Titus, R. Nanodisk-associated amphotericin B clears *Leishmania major* cutaneous infection in susceptible BALB/c mice. *Antimicrobial Agents and Chemotherapy* 50, 1238-1244, doi:10.1128/AAC.50.4.1238-1244.2006 (2006).
16. Nunes, M. C. *et al.* Chagas disease: an overview of clinical and epidemiological aspects. *Journal of the American College of Cardiology* 62, 767-776, doi:10.1016/j.jacc.2013.05.046 (2013).

17. Coura, J. R. & Borges-Pereira, J. Chagas disease: 100 years after its discovery. A systemic review. *Acta Tropica* 115, 5-13, doi:10.1016/j.actatropica.2010.03.008 (2010).
18. Bern, C. Antitrypanosomal therapy for chronic Chagas' disease. *The New England Journal of Medicine* 364, 2527-2534, doi:10.1056/NEJMct1014204 (2011).
19. Viotti, R. *et al.* Towards a paradigm shift in the treatment of chronic Chagas disease. *Antimicrobial Agents and Chemotherapy* 58, 635-639, doi:10.1128/AAC.01662-13 (2014).
20. Molina, I. *et al.* Randomized trial of posaconazole and benznidazole for chronic Chagas' disease. *The New England Journal of Medicine* 370, 1899-1908, doi:10.1056/NEJMoa1313122 (2014).
21. Morillo, C. A. *et al.* Randomized trial of benznidazole for chronic Chagas' cardiomyopathy. *The New England Journal of Medicine* 373, 1295-1306, doi:10.1056/NEJMoa1507574 (2015).
22. Viotti, R. *et al.* Side effects of benznidazole as treatment in chronic Chagas disease: fears and realities. *Expert Review of Anti-Infective Therapy* 7, 157-163, doi:10.1586/14787210.7.2.157 (2009).
23. Khare, S. *et al.* Antitrypanosomal treatment with benznidazole is superior to posaconazole regimens in mouse models of Chagas disease. *Antimicrobial Agents and Chemotherapy* 59, 6385-6394, doi:10.1128/AAC.00689-15 (2015).
24. Bustamante, J. M., Bixby, L. M. & Tarleton, R. L. Drug-induced cure drives conversion to a stable and protective CD8+ T central memory response in chronic Chagas disease. *Nature Medicine* 14, 542-550, doi:10.1038/nm1744 (2008).
25. Myburgh, E. *et al.* In vivo imaging of trypanosome-brain interactions and development of a rapid screening test for drugs against CNS stage trypanosomiasis. *PLoS Neglected Tropical Diseases* 7, e2384, doi:10.1371/journal.pntd.0002384 (2013).
26. Li, H. *et al.* Structure- and function-based design of *Plasmodium*-selective proteasome inhibitors. *Nature* 530, 233-236, doi:10.1038/nature16936 (2016).

27. Steverding, D. & Wang, X. Trypanocidal activity of the proteasome inhibitor and anti-cancer drug bortezomib. *Parasites & Vectors* 2, 29, doi:10.1186/1756-3305-2-29 (2009).

28. Ivens, A. C. *et al.* The genome of the kinetoplastid parasite, *Leishmania major*. *Science* 309, 436-442, doi:10.1126/science.1112680 (2005).

29. Li, X. *et al.* Effect of noncompetitive proteasome inhibition on bortezomib resistance. *Journal of the National Cancer Institute* 102, 1069-1082, doi:10.1093/jnci/djq198 (2010).

30. Fernandez, Y. *et al.* Chemical blockage of the proteasome inhibitory function of bortezomib: impact on tumor cell death. *The Journal of Biological Chemistry* 281, 1107-1118, doi:10.1074/jbc.M511607200 (2006).

References to the Methods section

31. Zhang, X., Goncalves, R. & Mosser, D. M. The isolation and characterization of murine macrophages. *Curr. Protoc. Immunol.* Chapter 14, Unit1 4.1 (2008).

32. Khare, S. *et al.* Utilizing chemical genomics to identify cytochrome b as a novel drug target for Chagas disease. *PLoS Pathogens* 11, e1005058, doi:10.1371/journal.ppat.1005058 (2015).

33. Buckner, F. S., Verlinde, C. L., La Flamme, A. C. & Van Voorhis, W. C. Efficient technique for screening drugs for activity against *Trypanosoma cruzi* using parasites expressing beta-galactosidase. *Antimicrobial Agents and Chemotherapy* 40, 2592-2597 (1996).

34. Logan-Klumpler, F. J. *et al.* GeneDB--an annotation database for pathogens. *Nucleic Acids Research* 40, D98-108, doi:10.1093/nar/gkr1032 (2012).

35. Taylor, M. C. & Kelly, J. M. pTcINDEX: a stable tetracycline-regulated expression vector for *Trypanosoma cruzi. BMC Biotechnology* 6, 32, doi:10.1186/1472-6750-6-32 (2006).

271 36. Hariharan, S., Ajioka, J. & Swindle, J. Stable transformation of *Trypanosoma cruzi*: inactivation of
272 the PUB12.5 polyubiquitin gene by targeted gene disruption. *Molecular and Biochemical*
273 *Parasitology* 57, 15-30 (1993).
274 37. Wirtz, E., Leal, S., Ochatt, C. & Cross, G. A. A tightly regulated inducible expression system for
275 conditional gene knock-outs and dominant-negative genetics in *Trypanosoma brucei*. *Molecular and*
276 *Biochemical Parasitology* 99, 89-101 (1999).
277 38. Wilk, S. & Chen, W.-E. Purification of the eukaryotic 20S proteasome. *Curr. Protoc. Protein Sci.*
278 Chapter 21 (2001).
279 39. Unno, M. *et al.* The structure of the mammalian 20S proteasome at 2.75 A resolution. *Structure* 10,
280 609-618 (2002).
281 40. Melnick, J. S. *et al.* An efficient rapid system for profiling the cellular activities of molecular
282 libraries. *Proceedings of the National Academy of Sciences of the United States of America* 103,
283 3153-3158, doi:10.1073/pnas.0511292103 (2006).
284 41. Waters, N. J., Jones, R., Williams, G. & Sohal, B. Validation of a rapid equilibrium dialysis approach
285 for the measurement of plasma protein binding. *Journal of Pharmaceutical Sciences* 97, 4586-4595,
286 doi:10.1002/jps.21317 (2008).
287 42. Wang, J. & Skolnik, S. Recent advances in physicochemical and ADMET profiling in drug
288 discovery. *Chemistry & Biodiversity* 6, 1887-1899, doi:10.1002/cbdv.200900117 (2009).
289 43. Kalvass, J. C., Tess, D. A., Giragossian, C., Linhares, M. C. & Maurer, T. S. Influence of microsomal
290 concentration on apparent intrinsic clearance: implications for scaling in vitro data. *Drug Metabolism*
291 *and Disposition: the Biological Fate of Chemicals* 29, 1332-1336 (2001).

44. Li, C. *et al.* A modern in vivo pharmacokinetic paradigm: combining snapshot, rapid and full PK approaches to optimize and expedite early drug discovery. *Drug Discovery Today* 18, 71-78, doi:10.1016/j.drudis.2012.09.004 (2013).
45. Sacks, D. L. & Melby, P. C. Animal models for the analysis of immune responses to leishmaniasis. *Curr. Protoc. Immunol.* Chapter 19, Unit 19.12 (2001).
46. McLatchie, A. P. *et al.* Highly sensitive in vivo imaging of *Trypanosoma brucei* expressing "red-shifted" luciferase. *PLoS Neglected Tropical Diseases* 7, e2571, doi:10.1371/journal.pntd.0002571 (2013).

FIGURE LEGENDS

Figure 1: **Chemical evolution of GNF6702 from the phenotypic hit GNF5343.** *L. donovani*: amastigotes proliferating within primary mouse macrophages; *T. brucei*: the bloodstream form trypomastigotes; *T. cruzi*: amastigotes proliferating in 3T3 fibroblast cells; macrophage: mouse primary peritoneal macrophages; EC_{50} and CC_{50}: half-maximum growth inhibition concentration; F: oral bioavailability in mouse after administering single compound dose (20 mg/kg) as a suspension; CL: plasma clearance in mouse after single iv bolus dose (5 mg/kg); N.D.: not determined; all EC_{50} and CC_{50} values correspond to means ± s.e.m. (n=4 technical replicates).

Figure 2: GNF6702 clears parasites in mouse models of kinetoplastid infections. a, Post-treatment *L. donovani* liver burdens in mouse model of VL as assessed by qPCR (n=5 mice). **b,** PK/PD relationship for ten GNF6702 analogues, each administered at several doses; circles: mean liver burdens associated with individual compound regimens (30 regimens in total; n=5 mice per regimen) relative to vehicle; horizontal dotted line: 90% reduction in the liver *L. donovani* burden; vertical dotted line: 0.94-fold multiple of the mean free compound plasma concentration/ the *L. donovani* EC_{90} value ratio. **c,** Post-treatment *L. major* footpad burdens in the BALB/c mouse model of CL as assessed by qPCR (n= 6 mice);

the p values (two-tailed distribution) relate parasite burdens in compound-treated mice with those from vehicle-treated mice; left inset picture: a representative mouse footpad after treatment with vehicle; right inset picture: a representative mouse footpad after treatment with GNF6702 10 mg/kg twice-daily regimen. **d,** *T. cruzi* burden in mouse blood (circles), colon (triangles) and heart (diamonds) as assessed by qPCR after 20 days of treatment and four weeks of immunosuppression (n=8 mice). **e,** Whole body *in vivo* imaging of bioluminescent *T. brucei* before and after treatment; *Trypanosoma brucei*–infected mice were treated by a single intraperitoneal injection of diminazene aceturate (n=3 mice) or by oral administration of GNF6702 once-daily for 7 days (n=6 mice); filled symbols show whole body bioluminescence values for individual mice; several mice from the untreated and diminazene aceturate-treated groups were euthanized between days 28 and 56 due to CNS infection symptoms; background bioluminescence values shown for uninfected mice (grey-filled squares; n=4) were collected independently from mice aged-matched for day 0 using the same acquisition settings. Red dotted lines in **a**, **c** and **d** plots show limit of parasite detection by qPCR; plot symbols below the red dotted line: mice with no detectable parasites; data points below the limit of detection are 'jittered' to show number of animals in a group; thick horizontal lines: means of the treatment groups; RU: relative units (parasite burden relative to the mean burden of the vehicle-treated group).

Figure 3: F24L mutation in proteasome beta 4 subunit confers selective resistance to GNF6702. a, growth inhibition of *T. cruzi* epimastigote strains ectopically expressing $PSMB4^{WT}$ or $PSMB4^{F24L}$ protein by GNF6702 and bortezomib; non-induced/induced: culture medium without/with tetracycline to modulate expression of tetracycline-inducible *PSMB4* genes. **b,** growth inhibition of *T. brucei* bloodstream form trypomastigotes constitutively overexpressing $PSMB4^{WT}$ or $PSMB4^{F24L}$ protein by GNF6702 and bortezomib. EC_{50} values for each strain/compound pair are listed inside **a** and **b** plot panels next to corresponding strain/compound symbol (defined in plot legends); means from n=3

technical replicates are shown; error bars represent s.e.m. values; for data points lacking error bars, s.e.m. values are smaller than circles representing means; due to limited aqueous solubility, the highest tested GNF6702 concentration was 10 μM. RU (relative units) in **a** and **b** corresponds to parasite growth relative to the DMSO control (%).

Figure 4: Compounds from GNF6702 series inhibit growth of kinetoplastid parasites by inhibiting parasite proteasome chymotrypsin-like activity. a, Inhibition of three proteolytic activities of purified wild type ($PSMB4^{WT}$) and $PSMB4^{I29M}$ *T. cruzi* proteasomes by GNF6702 and bortezomib; IC_{50} values for proteasome proteolytic activities are listed inside plots. **b,** Correlation between inhibition of chymotrypsin-like activity of purified *L. donovani* proteasome (IC_{50}) and *L. donovani* axenic amastigote growth inhibition (EC_{50}; data points correspond to means of 2 technical replicates); red circles: IC_{50}>20 μM; blue circles: EC_{50}>25 μM; yellow circles: IC_{50}>20 μM and EC_{50}>25 μM; data for 317 analogues are shown. **c,** Lineweaver-Burk plot of inhibition of *T. cruzi* proteasome chymotrypsin-like activity by GNF6702 at increasing concentrations of a peptide substrate. **d,** Effect of GNF6702 and bortezomib on three proteolytic activities of human constitutive proteasome; IC_{50} values for proteasome proteolytic activities are listed inside plots. Data shown in **a**, **c** and **d** represent means ± s.e.m. (n=3 technical replicates; for data points lacking error bars, s.e.m. values are smaller than circles representing means). Due to limited aqueous solubility, the highest tested GNF6702 concentration in experiments shown in **a** and **d** was 10 μM.

METHODS

Ethics statement for animal models. All procedures involving mice were performed in accordance with AAALAC standards or under UK Home Office regulations, and were reviewed and approved in accordance with the Novartis Animal Welfare Policy. Sample size was determined on the basis of the

minimum number of animals required for good data distribution and statistics. Blinding was not possible in these experiments but animals were selected randomly for each group.

Determination of IC_{50}, EC_{50} and CC_{50} values, and data correlation. Reported IC_{50}/ EC_{50}/ CC_{50} values were calculated by averaging IC_{50}/ EC_{50}/ CC_{50} values obtained from individual technical replicate experiments (n; specified in relevant Figure captions and Methods sub-sections). Each technical replicate experiment was performed on a different day with freshly prepared reagents. Reported standard errors of mean (s.e.m.) were calculated using IC_{50}/ EC_{50}/ CC_{50} values determined in individual technical replicate experiments. To calculate IC_{50}/ EC_{50}/ CC_{50} values, measured dose response values were fitted with 4-parameter logistic function y=A+(B-A)/(1+(x/C)^D) (model 201, XLfit, IDBS), where x refers to compound concentration and y corresponds to an assay readout value.

VL efficacy data for ten GNF6702 analogues (Fig. 2a) were fitted with 4-parameter logistic function y=A+(B-A)/(1+(x/C)^D) (model 201, XLfit, IDBS), where x values correspond to free mean compound plasma concentrations and y values correspond to $\log_{10}$(*L. donovani* liver burden).

To correlate parasite proteasome inhibition with parasite growth inhibition (Fig. 4b and Extended data Fig. 5), we fitted data with y=a*x+b function using the least square method (x corresponds to $\log_{10}(IC_{50})$; y corresponds to $\log_{10}(EC_{50})$).

***Leishmania donovani* axenic amastigote growth inhibition assay.** RPMI 1640 medium (HyClone) was supplemented with 20% heat-inactivated fetal bovine serum (Omega Scientific), 23 µM folic acid (Sigma-Aldrich), 100 µM adenosine (Sigma-Aldrich), 22 mM D-glucose (Sigma-Aldrich), 4 mM L-glutamine (Hyclone), 25 mM 2-(4-morpholino) ethanesulfonic acid (Sigma-Aldrich) and 100 IU penicillin/ 100 µg/mL streptomycin (HyClone), and adjusted to pH= 5.5 with 6 M hydrochloric acid (Fisher Scientific) at 37 °C. *Leishmania donovani* MHOM/SD/62/1S-CL2D axenic amastigotes were

cultured in 10 mL of this medium (Axenic Amastigote Medium) in T75 CELL-STAR flasks (Greiner Bio-One) at 37 °C/ 5% CO_2 and passaged once a week.

To determine compound growth inhibitory potency on *L. donovani* axenic amastigotes, 100 nL of serially diluted compounds in DMSO were transferred to the wells of white, solid bottom 384-well plates (Greiner Bio-One) by Echo 555 acoustic liquid handling system (Labcyte). Then, 1 x 10^3 of *L. donovani* axenic amastigotes in 40 µL of Axenic Amastigote Medium were added to each well, and plates were incubated for 48 hours at 37 °C/ 5% CO_2. Parasite numbers in individual plate wells were determined through quantification of intracellular ATP. The CellTiter-Glo luminescent cell viability reagent (Promega) was added to plate wells, and ATP-dependent luminescence signal was measured on an EnVision MultiLabel Plate Reader (Perkin Elmer). Luminescence values in wells with compounds were divided by the average luminescence value of the plate DMSO controls, and used for calculation of compound EC_{50} values as described above.

Axenic amastigote EC_{50} values shown in Fig. 4b correspond to means of 2 technical replicates.

Isolation and maintenance of *Leishmania donovani* splenic amastigotes. Female BALB/cJ mice (Envigo) infected with *L. donovani* MHOM/ET/67/HU3 (ATCC) for 50-80 days were euthanized, and infected spleens were removed and weighed. The weight of an infected spleen ranged from 300 to 600 mg. For comparison, spleens from non-infected age-matched BALB/cJ mice weighed ~100 mg. Infected spleens were washed in Axenic Amastigote Medium (composition described above) and placed into Falcon 50 mL conical centrifuge tubes (Fisher Scientific) containing ice-cold Axenic Amastigote Medium (15 mL per infected spleen). Spleens were homogenized on ice in a Dounce homogenizer and centrifuged at 200 x g for 15 minutes at 4 °C to remove tissue debris. *Leishmania donovani* amastigotes present in the supernatant were pelleted by centrifugation at 1,750 x g for 15 min at 4 °C and re-suspended either in Axenic Amastigote Medium (when used for *in vitro* macrophage infections) or in

405 Hanks' Balanced Salt Solution (when used for mouse infections; Hyclone). Suspensions of splenic
406 amastigotes were kept on ice and used for *in vitro* or *in vivo* infections within 2-3 hours. To propagate *L.*
407 *donovani* amastigotes *in vivo*, 6 to 7 weeks old female BALB/cJ mice were infected with 8 x 10^7 purified
408 splenic amastigotes in 200 µL of Hanks' Balanced Salt Solution by tail vein injection.
409 ***Leishmania donovani* intra-macrophage amastigote growth inhibition assay.** *In vitro* compound
410 potencies on intra-macrophage *L. donovani* MHOM/ET/67/HU3 were determined using primary murine
411 peritoneal macrophages infected with *L. donovani* splenic amastigotes. Primary macrophages were
412 elicited in female BALB/c mice for 72 hours following the injection of 500 µL of sterile aqueous 2%
413 starch (J. T. Baker) solution into the mouse peritoneal cavity. The protocol used for isolation of
414 peritoneal macrophages was described in detail previously[31]. The isolated macrophages were re-
415 suspended in Macrophage Infection Medium (RPMI-1640 medium supplemented with 2 mM L-
416 glutamine, 10% heat-inactivated fetal bovine serum, 10 mM sodium pyruvate (Hyclone), and 100 IU
417 penicillin/ 100 µg/mL streptomycin), and 50 µL of macrophage suspension (8 x 10^5 macrophages/mL)
418 were added to microscopy-grade, clear-bottom, black 384-well plates (Greiner Bio-One). Following
419 overnight incubation at 37 °C/ 5% CO_2, plate wells were washed with Macrophage Infection Medium to
420 remove non-adherent cells using ELx405 Select microplate washer (BioTek), and then filled with 40 µL
421 of Macrophage Infection Medium. *Leishmania donovani* HU3 splenic amastigotes isolated from infected
422 spleens were re-suspended in Macrophage Infection Medium at a concentration of 6 x 10^7 cells/mL, and
423 10 µL of the suspension were added to assay plate wells containing adherent macrophages. After a 24-
424 hour infection period at 37 °C/ 5% CO_2, plate wells were washed with Macrophage Infection Medium to
425 remove residual extracellular parasites and re-filled with 50 µL of the medium. *Leishmania donovani*-
426 infected macrophages were subsequently treated with DMSO-dissolved compounds (0.5% final DMSO
427 concentration in the assay medium) in dose response for 120 hours at 37 °C/ 5% CO_2. Next, treated

macrophages were washed with the phosphate-buffered saline buffer (PBS; Sigma-Aldrich) supplemented with 0.5 mM magnesium chloride (Sigma-Aldrich) and 0.5 mM calcium chloride (Sigma-Aldrich), fixed with 0.4% paraformaldehyde (Sigma-Aldrich) in PBS, permeabilized with 0.1% Triton X-100 (Sigma-Aldrich) in PBS, and stained with SYBR Green I nucleic acid stain(Invitrogen, 1:100,000 dilution in PBS) overnight at 4 ^{o}C. Image collection and enumeration of macrophage cells and intracellular *L. donovani* amastigotes was performed using the OPERA QEHS automated confocal microscope system equipped with 20x water immersion objective (Evotec Technologies) and the OPERA Acapella software (Evotec Technologies) as described previously[32].

All reported intra-macrophage *L. donovani* EC_{50} values were calculated from at least 3 technical replicates (n= 3 or n= 4; specified in relevant Figure captions).

***Trypanosoma brucei* growth inhibition assay.** Bloodstream form *Trypanosoma brucei* Lister 427 parasites were continuously passaged in HMI-9 medium formulated from IMDM medium (Invitrogen), 10% heat-inactivated fetal bovine serum, 10% Serum Plus medium supplement (SAFC Biosciences), 1 mM hypoxanthine (Sigma-Aldrich), 50 µM bathocuproine disulfonic acid (Sigma-Aldrich), 1.5 mM cysteine (Sigma-Aldrich), 1 mM pyruvic acid (Sigma-Aldrich), 39 µg/mL thymidine (Sigma-Aldrich), and 14 µL/L beta-mercapthoethanol (Sigma-Aldrich); all concentrations of added components refer to those in complete HMI-9 medium. The parasites were cultured in 10 mL of HMI-9 medium in T75 CELL-STAR tissue culture flasks at 37 °C/ 5% CO_2.

To determine compound growth inhibitory potency on *T. brucei* bloodstream form parasites, 100 nL of serially diluted compounds in DMSO were transferred to the wells of white, solid bottom 384-well plates (Greiner Bio-One) by Echo 555 acoustic liquid handling system. Then, 5 x 10^3 of *T. brucei* parasites in 40 µL of HMI-9 medium were added to each well, and the plates were incubated for 48 hours at 37 °C/ 5% CO_2. Parasite numbers in individual plate wells were determined through quantification of intracellular

ATP amount. The CellTiter-Glo luminescent cell viability reagent was added to plate wells, and ATP-dependent luminescence signal was measured on an EnVision MultiLabel Plate Reader. Luminescence values in wells with compounds were divided by the average luminescence value of the plate DMSO controls, and used for calculation of compound EC_{50} values as described above.

Trypanosoma brucei EC_{50} values shown in Fig. 1 and Extended Data Fig. 3 correspond to means of 4 technical replicates.

***Trypanosoma cruzi* amastigote growth inhibition assay.** NIH 3T3 fibroblast cells (ATCC) were maintained in RPMI 1640 medium (Life Technologies) supplemented with 10% heat-inactivated fetal bovine serum and 100 IU penicillin/ 100 µg/mL streptomycin at 37 °C/ 5% CO_2. *Trypanosoma cruzi* Tulahuen parasites constitutively expressing *Escherichia coli* beta-galactosidase[33] were maintained in tissue culture as an infection in NIH 3T3 fibroblast cells. Briefly, 2 x 10^7 *T. cruzi* trypomastigotes were used to infect 6 x 10^5 NIH 3T3 cells growing in T75 CELL-STAR tissue culture flasks and cultured at 37 °C/ 5% CO_2 until proliferating intracellular parasites lysed host 3T3 cells and were released into the culture medium (typically 6-7 days). During the infection, the tissue culture medium was changed every two days. Number of *T. cruzi* trypomastigotes present in one mL of medium was determined using a hemocytometer.

To determine compound potency on intracellular *T. cruzi* amastigotes, NIH 3T3 cells were re-suspended in phenol red-free RPMI 1640 medium containing 3% heat-inactivated fetal bovine serum and 100 IU penicillin/ 100 µg/mL streptomycin, seeded at 1,000 cells/ well (40 µL) in white, clear bottom 384-well plates (Greiner Bio-One), and incubated overnight at 37 °C/ 5% CO_2. The following day, 100 nL of each compound in DMSO were transferred to individual plate wells by Echo 555 acoustic liquid handling system. After one hour incubation, 1 x 10^6 of tissue culture-derived *T.cruzi* trypomastigotes, in 10 µL of phenol red-free RPMI 1640 medium supplemented with 3% heat-inactivated fetal bovine serum and 100

IU penicillin/ 100 µg/mL streptomycin were added to each well. Plates were then incubated for 6 days at 37 °C/ 5% CO_2. Intracellular *T. cruzi* parasites were quantified by measuring the activity of parasite-expressed beta-galactosidase. Ten microliters of a chromogenic beta-galactosidase substrate solution (0.6 mM chlorophenol red-β-D-galactopyranoside/ 0.6% NP-40 in PBS; both reagents from Calbiochem) were added to each well and incubated for 2 hours at room temperature. After incubation, absorption was measured at 570 nM on SpectraMax M2 plate reader (Molecular Devices). Measured absorbance values in wells with compounds were divided by the average absorbance value of the plate DMSO controls, and used for calculation of compound EC_{50} values as described above.

Trypanosoma cruzi amastigote EC_{50} values shown in Fig. 1 and Extended Data Fig. 3 correspond to means of 4 technical replicates.

***Trypanosoma cruzi* epimastigote proliferation assay.** *Trypanosoma cruzi* CL epimastigotes were continuously passaged in LIT medium containing 9 g/L liver infusion broth (Difco), 5 g/L bacto-tryptose (Difco), 1 g/L sodium chloride, 8 g/L dibasic sodium phosphate (Sigma-Aldrich), 0.4 g/L potassium chloride (Sigma-Aldrich), 1 g/L D-glucose, 10 % heat-inactivated fetal bovine serum and 10 ng/mL of hemin (Sigma-Aldrich). The medium was adjusted to pH= 7.2 with 6 M hydrochloric acid. The parasites were cultured in 10 mL of LIT medium in T75 CELL-STAR tissue culture flasks at 27 °C.

To determine compound growth inhibitory potency on *T. cruzi* epimastigotes, 100 nL of serially diluted compounds in DMSO were transferred to the wells of white, solid bottom 384-well plates (Greiner Bio-One) by an Echo 555 acoustic liquid handling system. Then, 5 x 10^3 of *T. cruzi* epimastigotes in 40 µL of LIT medium were added to each well, and the plates were incubated for 7 days at 27 °C. Parasite numbers in individual plate wells were determined through quantification of intracellular ATP amount. The CellTiter-Glo luminescent cell viability reagent was added to plate wells, and ATP-dependent luminescence signal was measured on an EnVision MultiLabel Plate Reader. Luminescence values in

wells with compounds were divided by the average luminescence value of the plate DMSO controls, and used for calculation of compound EC_{50} values as described above.

Trypanosoma cruzi epimastigote EC_{50} values shown in Extended Data Fig. 4 correspond to means of 3 technical replicates.

Mouse fibroblast NIH 3T3 growth inhibition assay. NIH 3T3 fibroblast cells were maintained in RPMI medium 1640 with glutamine (Life Technologies) supplemented with 5% heat-inactivated fetal bovine serum and 100 IU penicillin/ 100 µg/mL streptomycin (3T3 Medium) at 37 °C/ 5% CO_2. NIH 3T3 fibroblast cells were purchased from ATCC. We did not perform cell line authentication and did not test the cells for mycoplasma contamination. This cell line is not listed in the database of commonly misidentified cell lines maintained by ICLAC and NCBI Biosample.

To determine compound potency, NIH 3T3 cells re-suspended in 3T3 medium were seeded at 1,000 cells/ well (50 µL) in white 384-well plates (Greiner Bio-One) and incubated overnight at 37 °C/ 5% CO_2. The following day, 100 nL of each compound in DMSO were transferred to individual plate wells by Echo 555 acoustic liquid handling system and plates were incubated for five days at 37 °C/ 5% CO_2. Cell numbers in individual plate wells were determined through quantification of intracellular ATP amount. The CellTiter-Glo luminescent cell viability reagent was added to plate wells, and ATP-dependent luminescence signal was measured on an EnVision MultiLabel Plate Reader. Luminescence values in wells with compounds were divided by the average luminescence value of the plate DMSO controls, and used for calculation of compound CC_{50} values as described above.

NIH 3T3 CC_{50} values shown in Fig. 1 and Extended Data Fig. 3 correspond to means of 4 technical replicates.

Primary macrophage cytotoxicity assay. Primary macrophage cell viability was determined on mouse peritoneal macrophages infected with *L. donovani* and was expressed as the ratio of the number of

520 macrophage cells in wells treated with a compound to those in wells treated with DMSO. The number of
521 macrophage cells in wells was determined by high content microscopy as described previously[32].
522 All reported macrophage CC_{50} values were calculated from 4 technical replicates (n= 4; also specified in
523 Figure 1 and Extended Data Figure 3 captions).
524 **Selection of GNF3934- and GNF8000-resistant *T. cruzi* mutants.** *T. cruzi* epimastigotes cultures
525 resistant to GNF3943 and GNF8000 were generated using a methodology described previously[32]. Briefly,
526 epimastigotes were initially cultured in the presence of compound concentration equivalent to its
527 EC_{20} value (GNF3943 EC_{20}= 1.5 μM and GNF8000 EC_{20}= 0.2 μM in 0.2% DMSO) or 0.2% DMSO
528 (control). Once a week, parasites were counted and growth rates were determined. If the parasite cultures
529 exhibited a reduced growth rate compared to 0.2% DMSO-treated parasites, epimastigotes were cultured
530 at the same compound concentration. Once the growth rates matched that of the control epimastigote
531 culture (0.2% DMSO), parasites were transferred into medium containing two-fold higher compound
532 concentration. The process was repeated until significant resistance was achieved (~10- to 20-fold
533 increase in corresponding EC_{50} value). The time required for generation of cultures with such a level of
534 resistance was approximately five months. Resistant clones were isolated via cloning by limiting dilution,
535 and two independent clones were analyzed by whole genome sequencing.
536 ***T. cruzi* whole genome sequencing**. Chromosomal DNA isolation from GNF3943- and GNF8000-
537 resistant *T. cruzi* clones, whole genome sequencing and sequence analysis were performed as described
538 previously[32]. Sequencing reads were aligned to the *T. cruzi* CL Brenner genome[34].
539 **Generation of *T. cruzi* strains ectopically expressing proteasome beta 4 subunit variants.** *PSMB4*
540 TcCLB503891.100 was amplified from *T. cruzi* CL Brenner genomic DNA using KOD Hot Start DNA
541 Polymerase (EMD Millipore), and sense (5'-AAAGCGGCCGCATGTCGGAGACAACCATTG-3) and
542 antisense (5-CCATGATCTTGATGTAATATAAGGCATTCAGCCCTGCTG-3) primers. The

543 *PSMB4*^{F24L} gene was generated from the wild type *PSMB4* construct by site-directed mutagenesis using
544 mutagenic sense (5-CAGCAGGGCTGAATGCCTTATATTACATCAAGATCATGG-3') and antisense
545 (5'-CCATGATCTTGATGTAATATAAGGCATTCAGCCCTGCTG-3') primers and QuikChange II
546 Site-Directed Mutagenesis Kit (Stratagene). The sequences of the wild type and mutant *PSMB4* genes
547 were verified by sequencing and both gene versions were subcloned into the *T. cruzi* expression vector
548 pTcIndex1 under control of a T7 promoter[35]. *Trypanosoma cruzi* CL Brenner epimastigotes were first
549 transfected as described previously[36] with the pLEW13 plasmid[37] harboring a tetracycline-inducible T7
550 RNA polymerase gene. Transfected epimastigotes were selected in medium supplemented with neomycin
551 (G418) at 500 µg/ml, and then transfected a second time with either pTcIndex1-*PSMB4*^{wt} or pTcIndex1-
552 *PSMB4*^{F24L} plasmid. Double transfected epimastigotes were selected in the presence of 500 µg/mL of
553 G418 (Sigma-Aldrich) and 500 µg/mL of hygromycin (Sigma-Aldrich). Susceptibility of double
554 transfected epimastigote cell lines to compounds was assessed using induced (+5 mg/mL of tetracycline)
555 and non-induced parasite cultures after five days of compound treatment. Parasite viability was
556 determined with AlamarBlue (ThermoFisher Scientific).
557 Reported EC_{50} values for *T. cruzi* epimastigotes ectopically expressing PSMB4 proteins were calculated
558 from 3 technical replicates (n= 3; also specified in the Figure 3a caption).
559 **Generation of *T. brucei* strains ectopically expressing proteasome beta 4 subunit variants.** *PSMB4*
560 (Tb927.10.4710) was amplified from *T. brucei* Lister 427 genomic DNA using PCR SuperMix High
561 Fidelity (Invitrogen), sense (5'-GCAAGCTTATGGCAGAGACGACTATCGG-3) and antisense (5'-
562 GCGGATCCCTAGCTTACAGATTGCACTC-3') primers. The *PSMB4*^{F24L} gene was generated from the
563 wild type PSMB4 construct by site-directed mutagenesis using mutagenic sense (5'-
564 gctgcggggttaaatgcgttatactacattaagataacgg-3'), antisense (5'-ccgttatcttaatgtagtataacgcatttaaccccgcagc-3')
565 primers and QuikChange II Site-Directed Mutagenesis Kit (Stratagene). The sequences of the wild type

and mutant *PSMB4* genes were verified by sequencing and both gene versions were cloned into the *T. brucei* expression vector pHD1034 under control of a ribosomal RNA promoter. Transfected *T. brucei* Lister 427 cells were selected in medium supplemented with puromycin at 1 µg/ml. Susceptibility of transfected *T. brucei* cell lines to compounds were assessed after 2 days of compound treatment. Parasite viability was determined with CellTiter-Glo.

Reported EC_{50} values for *T. brucei* parasites ectopically expressing PSMB4 proteins were calculated from 3 technical replicates (n= 3; also specified in the Figure 3b caption).

Purification of parasite 20S proteasomes. *T. cruzi* CL epimastigotes, *L. donovani* MHOM/SD/62/1S-CL2D axenic amastigotes and *T. brucei* Lister 27 bloodstream form trypomastigotes were grown to log phase and harvested by centrifugation. The corresponding cell pellets were stored at -80 °C until further use. Prior to purification, 10 g of cell pellets were thawed, re-suspended in lysis buffer (50 mM Tris-HCl pH = 7.5, 1 mM TCEP, 5 mM EDTA, and 10 µM E-64), and lysed by passing cell suspension three times through a needle (22 gauge) and by subsequent three freeze/ thaw cycles. The lysate was first cleared of cellular debris by two centrifugation steps (15,000 x g at 4 °C for 15 minutes followed by 40,000 x g at 4 °C for 60 minutes) and then fractionated through ammonium sulfate precipitation. The protein fraction precipitated between 45% and 65% of ammonium sulfate saturation was re-suspended in 25 mM Tris-HCl pH = 7.5, 1 mM TCEP buffer, and dialyzed overnight at 4 °C against the same buffer. Proteasomes were further purified by anion exchange chromatography (Resource Q column, GE Healthcare Life Sciences) and size exclusion chromatography (Superose 6 column, GE Healthcare Life Sciences) as described elsewhere[38]. Active fractions from the latter purification step were pooled and used in proteasome biochemical assays.

Subunit composition analysis of purified *T. cruzi* 20S proteasome by LC/MS/MS. Purified *T. cruzi* proteasome sample was buffer-exchanged and concentrated into 100 mM trimethylamine bicarbonate-

589 HCl pH= 8.0, 150 mM NaCl buffer using a 10 kDa molecular weight cut-off micro-concentrator
590 (Milipore Amicon Ultra). The resulting proteasome sample (200 µl, 1 mg/ml) was mixed with 5 µl of a
591 TMTsixplex reagent (Pierce). After 60 second incubation to label primary amines, the reaction was
592 stopped by adding 25 µl of 5% hydroxylamine. The labeled sample was run on 4-20% Bis-Tris PAGE gel
593 (Invitrogen) to separate polypeptides. The gel was stained with eStain 2.0 (GenScript). Stained protein
594 bands were cut out and in-gel digested separately with elastase (Promega) and asparaginase (Roche).
595 Peptides generated by the digestions were resolved by HPLC using a vented column setup with a 2 cm
596 Poros 10 R2 (Life Technologies, Carlsbad, CA) self-packed pre-column, and a PepMap Easy-Spray C18
597 analytical column (15 cm x 75 µm ID, Thermo Scientific). Resin-bound proteolytic fragments were
598 eluted with 2 to 40% acetonitrile / 0.1% formic acid operated at 300 nL/min for 120 min. Spectra of
599 eluted peptide species were determined by a column-coupled Q Exactive hybrid quadrupole orbitrap
600 mass spectrometer (Thermo Scientific). Proteome Discoverer v1.4 software (Thermo Scientific) was used
601 to search the *T.cruzi* genome[28] with identified spectra for presence of 20S proteasome subunits
602 (Supplementary Table 7). Search parameters included fixed carbamidomethyl modification of cysteine,
603 and variable oxidation of methionine, deamidation of asparagine, pyro-glu of N-terminal glutamine, and
604 TMT(6-plex) modification of lysine residues.
605 **Measuring proteasome proteolytic activities.** The activity of purified parasite and human 20S
606 proteasomes was monitored by measuring cleavage of various rhodamine-labelled fluorogenic substrates.
607 Purified 20S proteasomes were diluted in proteasome assay buffer (25 mM Tris-HCl pH 7.5, 1 mM
608 dithiothreitol (Sigma-Aldrich), 10 mM sodium chloride, 25 mM potassium chloride, 1 mM magnesium
609 chloride, 0.05% (w/v) CHAPS (Sigma-Aldrich) and 0.9% DMSO) at a final concentration of 162 nM
610 (parasite proteasomes) or 25 nM (human proteasome), and pre-incubated with compound (40 nL; 0.2%
611 final DMSO concentration) for 1 hour. Next, the following substrates (Biosynthan GmbH) were added at

612 3 µM final concentration to monitor specific proteolytic activities (Suc-LLVY-Rh110-dPro:
613 chymotrypsin-like activity; Ac-RLR-Rh110-dPro: trypsin-like activity; Ac-GPLD-Rh110-dPro: caspase-
614 like activity). The reaction was allowed to proceed for two hours at room temperature and fluorescence as
615 a measure of purified 20S proteasome activity was monitored using the EnVision® plate reader
616 (excitation at 485 nm/ emission at 535 nm). Km and Ki values were calculated using GraphPad Prism
617 (GraphPad Software) 'Non-competitive enzyme inhibition' function.
618 Data shown in Fig. 4a, 4c, 4d and Extended Data Table 3 represent means of 3 technical replicates (n= 3).
619 Data shown in Fig. 4b and Extended Data Fig. 5 represent means of 2 technical replicates (n= 2).
620 **Monitoring accumulation of ubiquitylated proteins in intact cells.** Growing *T. cruzi* epimastigotes
621 were seeded into 24-well tissue culture plate (1 x 10^7 cells/per well) in LIT medium and treated for 2-12
622 hours with DMSO (0.2%) or various concentrations of bortezomib and GNF6702 at 27 °C. Following the
623 treatment, parasites were collected by centrifugation (3,500 g for 6 minutes) and washed twice with
624 phosphate-buffered saline (PBS). Epimastigotes were lysed by resuspending washed cells in a buffer
625 containing 50 mM Tris-HCl pH= 7.4, 150 mM sodium chloride, 1% CHAPS, 20 µM E-64 (Sigma-
626 Aldrich), 10 mM EDTA(Sigma-Aldrich), 5 mM N-ethylmaleimide(Sigma-Aldrich), 1 mM
627 phenylmethylsulfonyl fluoride (Sigma-Aldrich), 10 µg/mL leupeptin (Sigma-Aldrich), 10 µg/mL
628 aprotinin (Sigma-Aldrich), and incubating the suspension on ice for 20 minutes. Cell lysates were cleared
629 by centrifugation at 21,000 g for 30 min at 4 °C.
630 For 3T3 cells, 2 x 10^5 cells/ well were seeded into 24-well tissue culture plates in RPMI medium 1640
631 supplemented with 10% heat-inactivated fetal bovine serum, and incubated overnight at 37 °C to allow
632 cells to attach. Attached cells were treated for 2 hours with DMSO (0.25%) or various concentrations of
633 bortezomib and GNF6702. Treated cells were washed twice with PBS and then lysed by incubating cells
634 in modified RIPA buffer (50 mM Tris-HCl pH= 7.4, 1% Triton X-100, 0.2% sodium dodecylsulfate, 1

635 mM EDTA, 1 mM phenylmethylsulfonyl fluoride, 5 µg/mL aprotinin, 5 µg/mL leupeptin) for 30 min at
636 4 °C. Cell lysates were cleared by centrifugation at 21,000 g for 30 min at 4 °C.
637 Protein concentration in cell extracts was determined with BCA assay (ThermoFisher), and 10 µg of cell
638 extracts were loaded on NuPAGE Novex 4-12% Bis-Tris gel (Invitrogen). After electrophoresis, resolved
639 proteins were transferred to nitrocellulose membrane. Ubiquitylated proteins were detected with
640 polyclonal anti-ubiquitin primary antibody (Proteintech, catalogue number 10201-2-AP) and rabbit anti-
641 mouse IgG-peroxidase antibody (Sigma-Aldrich, catalogue number A0545), and then imaged using ECL
642 Prime Western Blotting Detection Reagent (Amersham) on Chemidoc XR+ imaging system (BioRad).
643 Collected western blot images were quantified using Image Lab software (BioRad). Briefly, rectangles of
644 identical size and shape were drawn around each blot lane to include inside the shape all ubiquitylated
645 protein bands within 17 - 198 kDa molecular mass range. Next, integrated signal intensities within the
646 rectangles (reported by the Image Lab software) were used for calculation of EC_{50} values. Three
647 technical replicate experiments (n= 3) for each different dose response experiment (GNF6702 on *T. cruzi*
648 epimastigotes; GNF6702 on 3T3 cells; bortezomib on *T. cruzi* epimastigotes; bortezomib on 3T3 cells)
649 were performed.
650 ***Trypanosoma cruzi* proteasome modeling studies**. The homology model of *T. cruzi* 20S proteasome
651 was built using 'Prime' protein structure prediction program (Schrödinger) and X-ray structure of bovine
652 20S proteasome (pdb accession code 1IRU)[39] as the template. The model was subjected to restrained
653 minimization to relieve inter-chain clashes. 'SiteMap' program (Schrödinger) was used to identify
654 pockets on a protein surface suitable for small molecule binding. Flexible ligand docking was performed
655 using 'Glide 5.8' (Schrödinger). The grid box was centered in a middle of the identified pocket and
656 extended by 10 Å, with outer box extending additional 20Å. The ligand was docked using the standard

657 precision (SP) algorithm and scored using 'GlideScore' (Schrödinger). The GNF6702 GlideScore is
658 equal to -8.5.
659 **Receptor, enzyme and ion channel assays.** GNF6702 profiling was performed at 10 μM concentration
660 in a selectivity panel at Eurofins (www.eurofinspanlabs.com/Catalog/AssayCatalog/AssayCatalog.aspx).
661 Listed values % change in the assay readout relative to the DMSO control. To determine inhibition of a
662 subset of human tyrosine kinases by GNF6702, the inhibitor was profiled on a panel of Ba/F3 cell lines
663 expressing individual Tel-activated kinases as described previously[40]. All assays were performed as
664 single technical repeats.
665 **Determination of GNF6702 thermodynamic solubility.** The solubility of GNF6702 was assessed in a
666 high throughput thermodynamic solubility assay as described previously[41]. First, 25 μL of GNF6702
667 DMSO solutions were transferred to individual wells of a 96-well plate. DMSO was evaporated and 250
668 μL of 67 mM potassium phosphate buffer pH 6.8 were added to yield projected final compound
669 concentrations from 1 μM to 100 μM. The plate was sealed to prevent solvent loss and shaken for 24
670 hours at room temperature. The plate was then filtered to remove non-dissolved material. Concentration
671 of GNF6702 in individual plate wells was determined by measuring solution UV absorbance with
672 reference to a GNF6702 calibration curve.
673 **Determination of GNF6702 permeability in Caco-2 assay.** A 96-Multiwell Insert System (BD
674 Biosciences) was used for the Caco-2 cell culture and permeability assay as described previously[42]. Caco-
675 2 cells were seeded onto insert wells at a density of 1.48×10^5 cells per ml and allowed to grow for 19-23
676 days before assays. To measure both absorptive (apical to basolateral [A-B]) and secretory (basolateral to
677 apical [B-A]) compound transport, a solution of GNF6702 at 10 μM concentration in 0.5% DMSO were
678 added to donor wells. The plate was incubated at 37°C for 2 hours, with samples taken at the beginning

and end of the incubation from both donor and acceptor wells. The concentration of GNF6702 was determined by LC-MS/MS.

Apparent drug permeability (Papp) was calculated using the following equation:

$$Papp = dQ/dt * 1/(A*Cin)$$

where dQ/dt is the total amount of a test compound transported to the acceptor chamber per unit of time (nmol/s), A is the surface area of the transport membrane (0.0804 cm^2), Cin is the initial compound concentration in the donor chamber (10 µM), and Papp is expressed as cm/s).

Determination of human CYP450 inhibition by GNF6702. Extent of inhibition of major human CYP450 isoforms 2C9, 2D6 and 3A4 by GNF6702 was determined using pooled human liver microsomes and the known specific substrates of various CYP450 isoforms: diclofenac (5 µM), bufuralol (5 µM), midazolam (5 µM), and testosterone (50 µM). Probe substrate concentrations were used at concentrations equal to their reported Km values. The CYP450 inhibition assays with probe substrates diclofenac (2C9) or midazolam (3A4) were incubated at 37 °C for 5 to 10 minutes using a microsomal protein concentration of 0.05 mg/mL. Probe substrates bufuralol (2D6) and testosterone (3A4) were incubated at 37 °C for 20 minutes using microsomal concentration 0.5 mg/mL. The test concentrations of GNF6702 ranged from 0.5 to 25 µM in the presence of 1% DMSO. The reactions were initiated by adding NADPH (1 mM final concentration; Sigma-Aldrich) after a 5-min pre-incubation. Incubations were terminated by the addition of 300 µL of acetonitrile to 100 µL of a sample. No significant cytochrome P450 inhibition was observed. Extent of CYP450 isoform inhibition was determined by quantifying residual concentrations of individual CYP450 substrate probes at the end of reactions by LC/MS/MS.

Determination of GNF6702 *in vitro* metabolic stability. The intrinsic metabolic stability of GNF6702 was determined in mouse and human liver microsomes using the compound depletion approach and

LC/MS/MS quantification. The assay measured the rate and extent of metabolism of GNF6702 by measuring the disappearance of the compound. The assay determined GNF6702 *in vitro* half-life ($T^1/_2$) and hepatic extraction ratios (ER) as described previously[43]. GNF6702 was incubated for 30 minutes at 1.0 µM concentration in a buffer containing 1.0 mg/ mL liver microsomes. Samples (50 µL) were collected at 0, 5, 15 and 30 minutes and immediately quenched by addition of 150 µL of ice-cold acetonitrile/ methanol/water mixture (8/1/1). Quantification of GNF6702 in samples was performed by LC/MS/MS, and the *in vitro* intrinsic clearance was determined using the substrate depletion method. The intrinsic clearance, CLint was calculated using the following equation:

$$CLint = (0.693/ T^1/_2) *(V/ M) ,$$

where $T^1/_2$ is the *in vitro* half-life, V (µL) is the reaction volume, and M (mg) is the microsomal protein amount. Finally the hepatic extraction ratio is calculated as:

$$ER = CLh/Qh ,$$

where CLh = hepatic clearance, Qh = hepatic blood flow.

Clh was calculated using the following equation:

$$CLh = (Qh * fu * CLint)/(Qh + fu * CLint) ,$$

where fu = fraction unbound to protein (assumed to be 1).

Pharmacokinetic studies. An outline of various *in vitro* and *in vivo* DMPK assays used in this study for compound profiling was summarized previously[44]. The pharmacokinetic properties of GNF compounds and calculation of pharmacokinetic parameters was performed as described previously[23]. Mean compound plasma concentrations were calculated from fitted functions approximating compound plasma profile throughout 8 days of dosing. Blinding was not possible in these experiments.

Bioanalysis of GNF6702 in plasma. Plasma concentration of GNF6702 was quantified using a LC/MS/MS assay. Solution of 20 ng/mL of verapamil hydrochloride (Sigma-Aldrich) in

acetonitrile/methanol mixture (3/1 by volume), was used as an internal standard. Twenty microliters of plasma samples were mixed with 200 µl of internal standard solution. The samples were vortexed and then centrifuged in an Eppendorf Centrifuge 5810R (Eppendorf) at 4,000 rpm for 5 minutes at 4 °C to remove precipitated plasma proteins. The supernatants (150 µl) were transferred to a 96-well plate and mixed with 150 µl H_2O. The samples (10 µl) were then injected onto a Zorbax SB-C8 analytical column (2.1 x 30 mm, 3.5 µm; Agilent Technologies) and separated using a three step gradient (1^{st} step: 1.5 mL of 0.05% formic acid in 10% acetonitrile; 2^{nd} step: 0.5 mL of 0.05% formic acid in 100% acetonitrile; 3^{rd} step: 0.5 mL of 0.05% formic acid in 10% acetonitrile) at flow rate of 700 µl/min. GNF6702 and verapamil were eluted at retention time 1.19 and 1.17 minutes, respectively. The HPLC system, consisting of Agilent 1260 series binary pump (Agilent Technologies), Agilent 1260 series micro vacuum degasser (Agilent Technologies) and CTC PAL-HTC-xt analytics autosampler (LEAP Technologies) was interfaced to a SCIEX API 4000 triple quadrupole mass spectrometer (Sciex). Mass spectrometry analysis was carried out using atmospheric pressure chemical ionization (APCI) in the positive ion mode. GNF6702 (430.07 > 333.20) and verapamil (455.16 > 164.90) peak integrations were performed using AnalystTM 1.5 software (Sciex). The lower limit of quantification (LLOQ) in plasma was 1.0 ng/mL. Samples were quantified using seven calibration standards (dynamic range 1 – 5,000 ng/mL) prepared in plasma and processed as described above.

Formulation of study drugs for *in vivo* efficacy experiments. All compounds administered to mice during efficacy experiments were formulated as suspensions in distilled water containing 0.5% methylcellulose (Sigma-Aldrich) and 0.5% Tween 80 (Sigma-Aldrich). During a treatment course, each mouse received 0.2 ml of drug suspension per dose by oral gavage.

Mouse model of visceral leishmaniasis. Female BALB/c mice (Envigo; 6-8 weeks old) were infected by tail vein injection with 4 x 10^7 *L. donovani* MHOM/ET/67/HU3 splenic amastigotes (protocol number

748 P11-319). Seven days after infection, animals were orally dosed for eight days with vehicle (0.5%
749 methylcellulose/ 0.5% Tween 80, miltefosine (12 mg/kg once-daily; Sigma-Aldrich), or a GNF
750 compound (twice-daily). On the first day of dosing, three mice were used for collection of blood for PK
751 determination and euthanized afterwards. On the last day of dosing, PK samples were collected from
752 remaining five mice, which were also used for determination of compound efficacy (n= 5 mice per
753 group). Liver samples were collected from these five mice and *L. donovani* parasite burdens were
754 quantified by qPCR as follows. Total DNA was extracted from drug-treated mice livers using the
755 DNeasy Blood and Tissue Kit (Qiagen). Two types of DNA were quantified in parallel using the
756 TaqMan assay: *L. donovani* major surface glycoprotein gp63 (Ldon_GP63) and mouse GAPDH. *L.*
757 *donovani* GP63 DNA was quantified with the following set of primers:
758 TGCGGTTTATCCTCTAGCGATAT (forward), AGTCCATGAAGGCGGAGATG (reverse), and
759 TGGCAGTACTTCACGGAC (TaqMan MGB probe, 5′-FAM-labeled reporter dye, non-fluorescent
760 quencher). Mouse GAPDH DNA was quantified with the following set of primers:
761 GCCGCCATGTTGCAAAC (forward primer), CGAGAGGAATGAGGTTAGTCACAA (reverse
762 primer), and ATGAATGAACCGCCGTTAT (TaqMan MGB probe, 5′-FAM-labeled reporter dye, non-
763 fluorescent quencher). Each qPCR reaction (10 µL) included 5 µl of TaqMan Gene Expression Master
764 Mix (Life Technologies), 0.5 µL of a 20X primer/probe mix (Life Technologies), and 4.5 µL (50 ng) of
765 total DNA from liver samples. DNA amount was quantified using the Applied Biosystems 7900HT
766 instrument. *L. donovani* parasite burden (RU: relative units) was expressed as the abundance of *L.*
767 *donovani* GP63 DNA relative to the abundance of mouse GAPDH DNA.
768 **Mouse footpad model of cutaneous leishmaniasis.** *L. major* MHOM/SA/85/JISH118 metacyclic
769 promastigotes were generated and purified by the peanut agglutinin method as described elsewhere[45]. To
770 establish the *L. major* footpad infection, female BALB/c mice (Envigo; 6-8 weeks old; protocol number

771 P11-319) were injected with suspension of *L. major* metacyclic promastigotes (1 x 10^6 parasites in 50
772 µL) into each hind footpad. After eight days of infection, animals were dosed with vehicle, miltefosine
773 (30 mg/kg once-daily), or indicated regimens of GNF6702 for seven days (n=6 mice per group). The
774 progress of infection was monitored by measuring the size (length and thickness) of hind footpad
775 swelling using digital calipers. At the end of the study, the mice were euthanized, and the footpad tissues
776 were extracted and used for genomic DNA isolation with the DNeasy Blood and Tissue kit (Qiagen). The
777 *L. major* footpad burden was determined by qPCR quantification of kinetoplastid minicircle DNA
778 (forward primer: 5'-TTTTACACCTCCCCCCAGTTT-3'; reverse primer: 5'-
779 CCCGTTCATAATTTCCCGAAA-3'; Taqman MGB probe: 5'-AGGCCAAAAATGG-3', 5′-FAM [6-
780 carboxyfluorescein]-labeled reporter dye, non-fluorescent quencher). The amounts of mouse
781 chromosomal DNA in extracted samples were quantified in parallel qPCR using a glyceraldehyde-3-
782 phosphate dehydrogenase (GAPDH) TaqMan assay as described for mouse VL model above. *L. major*
783 burden in footpad was expressed as the ratio of kinetoplast minicircle DNA to mouse GAPDH. P values
784 for the between-groups differences in efficacies were calculated with a Student's paired t test with a two-
785 tailed distribution.
786 **Mouse model of Chagas disease.** Compound efficacy in mouse model of Chagas disease was
787 determined as described previously[23]. Female C57BL/6 mice (Envigo; 6-8 weeks old; protocol number
788 P11-316) were infected by intraperitoneal injection with 10^3 tissue culture-derived *T. cruzi* CL
789 trypomastigotes. Starting at 35 days after infection, the animals were dosed orally once-daily with 100
790 mg/kg benznidazole (Sigma-Aldrich) and indicated doses of GNF6702 (1, 3, and 10 mg/kg twice-daily,
791 n=8 per group) for 20 days. Ten days following the end of drug treatment, the mice underwent four
792 cycles of cyclophosphamide immunosuppression, each cycle lasting one week. During each
793 immunosuppression cycle, mice were dosed by oral gavage once-daily with 200 mg/kg

cyclophosphamide (suspension in 0.5% methylcellulose/ 0.5% Tween80 aqueous solution) on day 1 and day 4 of the cycle. After the fourth immunosuppression cycle, blood samples were collected from the orbital venous sinus of each mouse, mice were euthanized and heart and colon samples were collected. Samples from treated mice were used for extraction of total DNA using the High Pure PCR template preparation kit (Roche). The amounts of *T. cruzi* satellite DNA (195-bp fragment) in extracted DNA samples were quantified by real-time qPCR TaqMan assay (Life Technologies) with the following set of primers: AATTATGAATGGCGGGAGTCA (forward primer), CCAGTGTGTGAACACGCAAAC (reverse primer), and AGACACTCTCTTTCAATGTA (TaqMan MGB probe, 5′-FAM [6-carboxyfluorescein]-labeled reporter dye, non-fluorescent quencher). The amounts of mouse chromosomal DNA in extracted samples were quantified in parallel qPCR reactions using a GADPH (glyceraldehyde-3-phosphate dehydrogenase) TaqMan assay as described for mouse VL model above. Each qPCR mixture (10 µl) included 5 µl of TaqMan Gene Expression master mix (Life Technologies), 0.5 µl of a 20x primer/ probe mix (Life Technologies), and 4.5 µl (50 ng) of total DNA extracted from blood samples. PCRs were run on the Applied Biosystems 7900HT instrument. *T. cruzi* parasitemia was expressed as the abundance of *T. cruzi* microsatellite DNA relative to the abundance of mouse GAPDH DNA.

Mouse model of stage II HAT. Female CD1 (Charles River UK; ~8 weeks old; protocol number PPL 60/4442) mice were infected by injection into the peritoneum with 3 x 10^4 *T. brucei* (GVR35-VSL2) bloodstream form parasites[46]. Starting on day 21, mice were dosed by oral gavage once-daily with GNF6702 (n= 6) at 100 mg/kg for 7 days or a single dose of diminazene aceturate (Sigma-Aldrich) at 40 mg/kg in sterile water was administered by ip injection (n= 3). A group of untreated mice (n= 3) was included as controls.

Mice were monitored weekly for parasitemia from day 21 post-infection. *T. brucei* was quantified in blood samples from the tail vein by microscopy, and *in vivo* bioluminescence imaging of infected mice was performed before treatment on day 21 post-infection and in weeks following the treatment (day 28, 35, 42, 56, 63, 72, 84, 92 post-infection). Imaging on groups of three mice was performed 10 min after ip injection of 150 mg D-luciferin (Promega)/kg body weight (in PBS) using an IVIS Spectrum (PerkinElmer) as described previously[25]. A group of uninfected mice (aged-matched for day 0 time point; n= 4) were imaged using the same acquisition settings to show the background bioluminescence (Fig. 2e, grey-filled squares) in the absence of luciferase-expressing *T. brucei* after day 92 of the experiment. Untreated and diminazene-treated mice were euthanized on days 32 and 35, and day 42, respectively, due to high parasitemia or the development of symptoms related to CNS infection. GNF6702-treated mice were euthanized on day 92. No parasitemia or clinical symptoms were observed at this point. At the specified endpoints mice were sacrificed by cervical dislocation, after which whole brains were removed and imaged *ex vivo* within 10 minutes after administration of 100 µL of D-luciferin onto the brain surface. Data analysis for bioluminescence imaging was performed using Living Image Software. The same rectangular region of interest (ROI) covering the mouse body was used for each whole body image to show the bioluminescence in total flux (photons per second) within that region. Image panels of whole mouse bodies are composites of the original images with areas outside the ROI cropped out to save space. For *ex vivo* brain images the same oval shaped ROI was used to display the bioluminescence detected for each mouse brain at the respective endpoints.

Chemical synthesis. The detailed procedures for chemical synthesis are presented in Supplementary Information.

END NOTES

Supplementary Information can be found at the end of this manuscript.

Acknowledgements This work was supported in part by grants from the Wellcome Trust (091038/Z/09/Z to R.J.G. and F.S., and 104976/Z/14/Z, 104111/15/Z to J.C.M. and E.M.) and NIH (AI106850 to F.S.B.). We thank Simon Croft, Rob Don, Lars Gredsted, Alan Hudson and John Mendlein for discussions, Rick Tarleton for *T. cruzi* CL strain, and George Cross for *T.b. brucei* Lister 427 strain. We thank Andreas Kreusch for help with proteasome purification, and Fabio Luna for help with *T. cruzi* whole genome sequencing. We acknowledge technical assistance of Omeed Faghih in generating the plasmids for ectopic expression of *PSMB4* in *T. cruzi*, Ryan Ritchie for IVIS *in vivo* imaging, and Annie Mak, Jason Matzen and Paul Anderson for execution of high throughput screens. We thank John Isbell and Thomas Hollenbeck for profiling GNF6702 in ADME assays.

Contributions

A.B., F.L., C.J.N.M., P.K.M., A.S.N., J.L.T. and V.Y. designed chemical analogues, and performed chemical synthesis and purification of synthesized analogues. F.S.B., J.B., J.R.G., S.K., H.X.Y.K., Y.H.L., S.P.S.R., F.S., and X.L. conducted and analyzed data from *in vitro* growth inhibition assays. L.C.D., X.L., J.C.M., E.M., I.C.R., S.P.S.R., M.S., F.S., and B.G.W. conducted and analyzed data from *in vivo* efficacy assays. J.B., M.-Y.G., S.K., and F.S. conducted proteasome purification, proteasome inhibition assays and biochemical data analysis. S.W.B., G.F., S.K., F.S., and J.R.W. designed, conducted and analyzed experiments resulting in identification of proteasome resistance mutations. G.S. and B.B. built the homology model of *T. cruzi* proteasome structure and performed GNF6702 docking. A.B. and J.D.V. analyzed *T. cruzi* proteasome by mass spectrometry. A.N., T.G., M.S., F.S., and T.T. designed, conducted, and analyzed PK data. A.N. and V.M. led the chemistry team. F.S. led the biology team. R.J.G. and F.S. supervised and led the overall project, and led the writing of the manuscript. All authors contributed to writing of the manuscript.

Author affiliations

[1]Genomics Institute of the Novartis Research Foundation, San Diego, California 92121, USA. [2]Wellcome Trust Centre for Molecular Parasitology, Institute of Infection, Immunity and Inflammation, College of Medical, Veterinary and Life Sciences, University of Glasgow, Glasgow G12 8TA, UK. [3]Centre for Immunology and Infection, Department of Biology, University of York, Wentworth Way, Heslington, York, YO10 5DD, UK. [4]Department of Medicine, University of Washington, Seattle, Washington 98109, USA. [5]Novartis Institute for Tropical Diseases, Singapore.

Author information

*These authors contributed equally to this work.

Competing financial interests

Patents related to this work has been filed (WO 2015/095477 A1, WO 2014/151784 A1, WO 2014/151729). Several authors own shares of Novartis.

Corresponding authors

Correspondence and requests for materials should be addressed to F. S. (fsupek@gnf.org)

EXTENDED DATA LEGENDS

Extended Data Figure 1: Pharmacokinetic profile of GNF6702 in mouse. a, Time profiles of mean free plasma concentration of GNF6702 in mouse model of visceral leishmaniasis; free GNF6702 concentration values were predicted from measured total plasma concentration values collected on day 1 and day 8 of treatment. Dashed blue lines correspond to intra-macrophage *L. donovani* EC_{50} of 18 ± 1.8 nM and EC_{99} of 42 ± 5.6 nM. Circles: means ± s.d.; n=3 mice for treatment day 1; n=5 mice for treatment day 8; fraction unbound in mouse plasma=0.063. For data points lacking error bars, standard deviations are smaller than circles representing means. **b,** Time course of total GNF6702 concentration in mouse plasma and brain after single oral dose (20 mg/kg); n=2 mice per time point; circles: measured values; rectangles: means.

Extended Data Figure 2: GNF6702 clears parasites from mice infected with *T. brucei*. a, *In vivo* quantification of bioluminescent *T. brucei* in infected mice before and after treatment. ip: intraperitoneal; day 21: start of treatment; day 28: 24 hours after last GNF6702 dose; day 42: evaluation of early parasite recrudescence in mice treated with diminazene aceturate (n=3); day 42 and 92: absence of parasite recrudescence in mice treated with GNF6702 (n=6). Images from uninfected mice (3 mice of 4 are shown) aged-matched for day 0 were collected independently using the same acquisition settings. Parasitemia (blue font) and whole mouse total flux (black font) values of each animal are shown above the image; N.D.: not detectable. Within each group the mouse numbers in yellow (top left in each image) refer to the same mouse imaged throughout. Complete sets of parasitemia and whole mouse total flux values collected on individual mice throughout the experiment are listed in Supplementary Tables 4 and 5. **b,** Brains from mice shown in panel a were soaked in luciferin and imaged for presence of bioluminescent *T. brucei* at the indicated time points. For three diminazene-treated mice, two images of each brain are shown, one at a lower sensitivity (left) and the other at a high signal intensity scale.

Extended Data Figure 3: Structures and profiles of GNF3943 and GNF8000 used for selection of resistant *T. cruzi* lines. *L. donovani*: amastigotes proliferating within primary mouse macrophages; *T. brucei*: the bloodstream form trypomastigotes; *T. cruzi*: amastigotes proliferating in 3T3 fibroblast cells; macrophage: mouse primary peritoneal macrophages; EC_{50} and CC_{50} : half-maximum growth inhibition concentration; F: oral bioavailability in mouse after administering single compound dose (20 mg/kg) as a suspension; CL: plasma clearance in mouse after single iv bolus dose (5 mg/kg); all EC_{50} and CC_{50} values correspond to means ± s.e.m. (n=4 technical replicates).

Extended Data Figure 4: Mutations in proteasome beta 4 subunit confer resistance to GNF6702 in *T. cruzi* and *T. brucei*. a, growth curves of wild type, GNF3943-resistant and GNF8000-resistant *T. cruzi* epimastigote strains in the presence of increasing concentrations of GNF6702, nifurtimox,

bortezomib and MG132; RU (relative units) corresponds to parasite growth relative to the DMSO control (%); for data points lacking error bars, standard errors are smaller than circles representing means; due to limited aqueous solubility, the highest tested GNF6702 concentration was 10 µM. **b,** growth inhibition EC_{50} values of GNF6702, bortezomib, MG132 and nifurtimox on indicated *T. cruzi* strains. **c,** growth inhibition EC_{50} values of GNF6702 and bortezomib on *T. cruzi* epimastigotes and *T. brucei* bloodstream form trypomastigotes overexpressing $PSMB4^{WT}$ or $PSMB4^{F24L}$. Data shown in panels **a**, **b** and **c** correspond to means ± s.e.m. (n=3 technical replicates).

Extended Data Figure 5: Correlation between inhibition of parasite proteasome chymotrypsin-like activity and parasite growth inhibition by the GNF6702 compound series. IC_{50}: half-maximum inhibition of indicated parasite proteasome; *T. brucei* EC_{50}: half-maximum growth inhibition on *T. brucei* bloodstream form trypomastigotes; *T. cruzi* EC_{50}: half-maximum growth inhibition on *T. cruzi* amastigotes proliferating inside 3T3 cells; data points correspond to means of 2 technical replicates; red circles: IC_{50}>20 µM; yellow circles: IC_{50}>20 µM and EC_{50}>25 µM; data for 317 analogues are shown.

Extended Data Figure 6: Hypothetical model of GNF6702 binding to *T. cruzi* proteasome beta 4 subunit. a, Alignment of amino acid sequences of proteasome beta 4 subunits (PSMB4) from *L. donovani*, *T. cruzi*, *T. brucei and H. sapiens*. Green: amino acid residues conserved between human and kinetoplastid PSMB4 proteins; blue: amino acid residues conserved only among kinetoplastid PSMB4 proteins; black: amino acids mutated in *T. cruzi* mutants resistant to analogues from the GNF6702 series. **b,** Surface representation of the modeled *T. cruzi* 20S proteasome structure showing relative positions of the beta 5 and beta 4 subunits. Beta 4 amino acid residues F24 and I29 (colored yellow) are located at the interface of the two beta subunits. GNF6702 is depicted in a sphere representation bound into a predicted pocket on the beta 4 subunit surface with carbon, nitrogen, oxygen and hydrogen atoms colored magenta, blue, red and grey, respectively. The other *T. cruzi* 20S proteasome subunits are colored gray. **c,** Close-up

of the beta 5 and beta 4 subunits. The beta 5 subunit active site (pocket 1, chymotrypsin-like activity) is colored pale green. The predicted beta 4 pocket (pocket 2) with bound GNF6702 is colored blue. The inhibitor is shown in a stick representation with atoms colored as described in caption for the b panel. Beta 4 residues F24 and I29 are colored yellow. The proteasome model shown in panels b and c was produced by The PyMol Molecule Graphics System, Version 1.8, Schrodinger, LLC.

Extended Data Figure 7: Effect of GNF6702 on accumulation of ubiquitylated proteins by *T. cruzi* epimastigotes and 3T3 cells. a, Western blot analysis of *T. cruzi* whole cell extracts with anti-ubiquitin antibody after treatment with GNF6702 and bortezomib. **b,** Western blot analysis of 3T3 whole cell extracts with anti-ubiquitin antibody after treatment with GNF6702 and borteomib. **c,** Concentrations of GNF6702 and bortezomib effecting half-maximum accumulation of ubiquitylated proteins in *T. cruzi* and 3T3 cells (means ± s.e.m.; n=3 technical replicates); total ubiquitin signal values in individual blot lanes shown in panels **a** and **b** were quantified and used for calculation of the listed EC_{50} values. In **a** and **b**, numbers above the blot lanes indicate compound concentrations and D indicates control, DMSO-treated cells. For western blot source data, see Supplementary Figure 1.

Extended Data Table 1: Point mutations identified by whole genome sequencing in GNF3943- and GNF8000-resistant *T. cruzi* epimastigotes.

Extended Data Table 2: Enzyme inhibition IC_{50} values of bortezomib and GNF6702 on three proteolytic activities of wild type *T. cruzi*, $PSMB4^{I29M}$ *T. cruzi*, and *H. sapiens* proteasomes.

Extended Data Table 3: Inhibition kinetics parameters of GNF6702 on *L. donovani* and *T. cruzi* proteasomes.

SUPPLEMENTARY METHODS

1. Genomics Institute of the Novartis Research Foundation (GNF) chemical library

The GNF chemical library consists of ~3 million low molecular weight compounds.

2. High throughput screening (HTS) campaigns and hit identification

The high throughput screens were performed using 1,536 well polystyrene solid bottom white microplates (Greiner Bio-One). The GNF chemical library was tested against *L. donovani*, *T. brucei* and *T. cruzi* in whole-cell growth inhibition screens at single compound concentrations specified in sections below describing individual parasite screens. Parasite proliferation protocols described in the Methods section were optimized for 1,536 well plate assay format to provide optimal assay window and Z-factor. Primary hits included compounds that reduced growth of parasites by more than 50% relative to the relevant DMSO controls.

2.1. *Leishmania donovani* HTS

Leishmania donovani MHOM/SD/62/1S-CL2D axenic amastigotes in cell suspension were dispensed into 1,536-well assay plates (2,000 parasite cells in 5 µL of medium) and library compounds dissolved in DMSO were added to 4 µM final concentration (0.4% final DMSO concentration). After 48 hour incubation at 37 ^{o}C, parasite viability was assessed using the CellTiter-Glo Luminescent Cell Viability Assay (Promega) as described previously[32]. Compounds causing more than 50% reduction in parasite viability were considered hits. Identified hits were subsequently evaluated in the screening assay in triplicates at 4 µM compound concentration. Compounds that inhibited *L. donovani* growth in at least two replicates were considered confirmed hits.

2.2. *Trypanosoma brucei* HTS

Trypanosoma brucei Lister 427 bloodstream trypomastigotes in cell suspension were dispensed into 1,536-well assay plates (900 parasite cells in 7 µL of medium) and library compounds dissolved in DMSO were added to 7 µM final concentration (0.7% final DMSO concentration). After 48 hour incubation at 37 ^{o}C, parasite viability was assessed using the CellTiter-Glo Luminescent Cell Viability Assay (Promega) as described previously[32]. Compounds causing more than 50% reduction in parasite

viability were considered hits. Identified hits were subsequently evaluated in the screening assay in triplicates at 7 μM compound concentration. Compounds that inhibited *T. brucei* growth in at least two replicates were considered confirmed hits.

2.3. *Trypanosoma cruzi* HTS

A suspension of mouse fibroblast 3T3 cells was dispensed into 1,536-well assay plates (750 cells in 5 μL of medium). After overnight incubation at 37 ^{o}C, adhered 3T3 cells were infected with *T. cruzi* trypomastigotes (2,500 trypomastigotes per well in 3 μL of medium) and library compounds dissolved in DMSO were added to 6.3 μM final concentration (0.63% final DMSO concentration). After an additional 96 hour incubation at 37 °C, parasite viability was assessed using the BetaGlo Luminiscent Assay (Promega) as described previously[32]. Compounds causing more than 50% reduction in parasite viability were considered hits. Because of a large number of screen hits, we further followed upon only on a small subset of hits that were also identified as confirmed hits in *L. donovani* and *T. brucei* high throughput screens. Out of 93 such hits, 77 compounds were confirmed to be selective pan-kinetoplastid inhibitors (*L. donovani*, *T. brucei*, *T. cruzi* EC_{50} values < 10 μM, selectivity index relative to 3T3 CC_{50}> 5).

3. Chemical synthesis

Unless otherwise noted, materials were obtained from commercial suppliers and were used without purification. Removal of solvent under reduced pressure refers to distillation using Büchi rotary evaporator attached to a vacuum pump (~3 mm Hg). Products obtained as solids or high boiling oils were dried under vacuum (~1 mm Hg). Purification of compounds by high pressure liquid chromatography was achieved using a Waters 2487 series with Ultra 120 5 μm C18Q column with a linear gradient from 10% solvent A (acetonitrile with 0.035% trifluoroacetic acid) in solvent B (water with 0.05% trifluoroacetic acid) to 90% A in four minutes, followed by two and half minute elution with 90% A.

^{1}H NMR spectra were recorded on Bruker XWIN-NMR (400 MHz or 600 MHz). Proton resonances are reported in parts per million (ppm) downfield from tetramethylsilane (TMS). ^{1}H NMR data are reported as multiplicity (s - singlet, d - doublet, t - triplet, q - quartet, quint - quintet, sept - septet, dd - doublet of doublets, dt - doublet of triplets, bs - broad singlet), number of protons and coupling constant in Hertz. For spectra obtained in $CDCl_3$, DMSO-d_6, CD_3OD, the residual protons (7.27, 2.50 and 3.31 ppm respectively) were used as the reference.

Analytical thin-layer chromatography (TLC) was performed on commercial silica plates (Merck 60-F 254, 0.25 mm thickness); compounds were visualized by UV light (254 nm). Flash chromatography was performed either by CombiFlash® (Separation system Sg. 100c, ISCO) or using silica gel (Merck Kieselgel 60, 230-400 mesh). Agilent 1100 series liquid chromatograph/ mass selective detector (LC/ MSD) was used to monitor the progress of reactions and check the purity of products using 254 nm and 220 nm wavelengths, and electrospray ionization (ESI) positive mode. Mass spectra were obtained in ESI positive mode. Elemental analyses were carried out by Midwest microlabs LLC, Indianapolis.

3.1. Synthesis of GNF5343

GNF5343 is a commercially available compound and was purchased from Chembridge laboratories (catalogue # 5840200).

3.2. Synthesis of GNF6702; N-(4-fluoro-3-(6-(pyridin-2-yl)-[1,2,4]triazolo[1,5-a]pyrimidin-2-yl)phenyl)-2,4-dimethyloxazole-5-carboxamide

3.2.1. Synthesis of 2-fluoro-5-nitrobenzoyl chloride (1)

A solution of 2-fluoro-5-nitrobenzoic acid (50 g, 270 mmol) in thionyl chloride (100 mL) was heated to 80 °C and stirred for 4 hours. The mixture was allowed to cool down to room temperature and the solvent was removed to give compound **1** (54 g, 98% yield).

3.2.2. Synthesis of 2-(2-fluoro-5-nitrobenzoyl)hydrazine-1-carboximidamide (2)

To a solution of aminoguanidine carbonate (36.2 g, 266 mmol) in dry toluene (300 mL) at 0 °C, was added compound **1** (54 g, 0.266 mol) over 30 minutes. The mixture was stirred at room temperature for 12 hours. The formed precipitate was removed by filtration, and the residue was treated with H_2O (400 mL) and made alkaline with sodium carbonate. The solid was collected and recrystallized from water to obtain compound **2** (62 g, 97% yield). M/Z 241.1 (M+1).

3.2.3. Synthesis of 5-(2-fluoro-5-nitrophenyl)-4H-1,2,4-triazol-3-amine (3)

A solution of compound **2** (62 g, 0.257 mol) in H_2O (800 mL) was stirred for 8 hours at 100 °C. After cooling, the obtained solid was filtered, and the cake was washed with H_2O (100 mL), tetrahydrofuran (100 mL), and dried to give compound **3** (34 g, 51% yield). ^{1}H NMR (400 MHz, DMSO) 12.42 (s, 1H), 8.74 (dd, *J* = 6.27, 3.01 , 1H), 8.26 (dt, *J* = 8.97, 3.42 , 1H), 7.57 (t, *J* = 9.54 , 1H), 6.29 (s, 2H).

3.2.4. Synthesis of 2-(2-fluoro-5-nitrophenyl)-6-(pyridin-2-yl)-[1,2,4]triazolo[1,5-a] pyrimidine (4)

To a solution of compound **3** (1 g, 4.48 mmol) in acetic acid (20 mL) 2-(pyridin-2-yl)malonaldehyde (0.8 g, 5.376 mmol) was added at room temperature. The mixture was heated to 100 °C and stirred for 4 hours. The mixture was allowed to cool to room temperature before adding water (50 mL), filtered, and the filter cake was washed with saturate sodium bicarbonate solution (100 mL), H_2O (100 mL), and tetrahydrofuran (100 mL) and dried under vacuum to give compound **4** (0.9 g, 60% yield). ^{1}H NMR (400 MHz, DMSO) 10.13 (d, *J* = 2.01 ,1H), 9.68 (d, *J* = 2.01 , 1H), 9.09- 9.02 (m, 1H), 8.77 (d, *J* = 4.27 , 1H), 8.28-8.19 (m, 1H), 8.15-7.96 (m, 2 H), 7.77 (t, *J* = 9.54 , 1H), 7.56-7.43 (m, 1H).

3.2.5. Synthesis of 4-fluoro-3-(6-(pyridin-2-yl)-[1,2,4]triazolo[1,5-a]pyrimidin-2-yl)aniline (5)

To a solution of compound **4** (0.15 g, 0.443 mmol) in tetrahydrofuran (5 mL) was added Raney Nickel (0.2 g) and ZnI_2 (71 mg) at room temperature. The mixture was stirred under H_2 (50 psi) at 25 °C for 2.5 hours. The mixture was diluted with methanol (10 mL) and filtered. The solvent was removed and the crude product was washed with methanol (5 mL x 2) and dried under vacuum to give compound **5** (90

mg, 66% yield). ^{1}H NMR (400 MHz, DMSO) 10.01-10.06 (m, 1H), 9.62-9.58 (m, 1H), 8.73-8.78 (m, 1H), 8.24-8.20 (m, 1H), 8-02-7.96 (m, 1H), 7.57-7.47 (m, 2H), 7.08-7.05 (m, 1H), 6.76-6.70 (m, 1H), 5.24 (s, 2H) M/Z 307.01 (M+1).

3.2.6. Synthesis of N-(4-fluoro-3-(6-(pyridin-2-yl)-[1,2,4]triazolo[1,5-a]pyrimidin-2-yl)phenyl)-2,4-dimethyloxazole-5-carboxamide (GNF6702; 6)

To a solution of 2,4-dimethyloxazole-5-carboxylic acid (40.6 mg, 0.28 mmol) in dimethylformamide (5 mL) was added HATU (118.6 mg, 0.31 mmol) and DIEA (72.4 mg, 0.56 mmol) at room temperature. The mixture was stirred for 30 min, the intermediate **5** (80 mg, 0.26 mmol) was added at room temperature. The mixture was stirred for 3 hours, water (10 mL) was added, the mixture was filtered, and the filter cake was washed with H_2O (5 mL x 2), tetrahydrofuran (5 mL x 2) and purified by HPLC to give product **6** (33 mg, 31% yield). ^{1}H NMR (400 M, MeOD) 9.84 (d, *J* = 2.4, 1H), 9.61 (d, *J* = 2.3, 1H), 8.76 (dt, *J* = 4.8, 1.4, 1H), 8.54 (dd, *J* = 6.4, 2.7, 1H), 8.12 (dt, *J* = 8.0, 1.1, 1H), 8.00 (td, *J* = 7.8, 1.8, 1H), 7.93 (ddd, *J* = 8.9, 4.1, 2.7, 1H), 7.49 (ddd, *J* = 7.5, 4.9, 1.0, 1H), 7.34 (dd, *J* = 10.4, 9.0, 1H), 2.57 (s, 3H), 2.48 (s, 3H). M/Z= 430.13 (M+1).

3.3. Synthesis of GNF3943; Isopropyl (2-(2-chloro-5-(furan-2-carboxamido)phenyl)-1H-imidazo[4,5-b]pyridin-6-yl)carbamate

3.3.1. Synthesis of 2-chloro-5-(furan-2-carboxamido)benzoic acid (7)

To a suspension of 5-amino-2-chlorobenzoic acid (13.7 g, 79.85 mmol, 1.00 equiv) in tetrahydrofuran (100 mL) was added furan-2-carbonyl chloride (11.5 g, 88.10 mmol, 1.10 equiv) at 0 °C. The ice bath was then removed and the reaction was stirred overnight at room temperature. The resulting mixture was concentrated under vacuum and diluted with DCM. The solid was collected by filtration to give 17 g (80%) of 2-chloro-5-(furan-2-amido)benzoic acid (**7**) as a gray solid.

3.3.2. Synthesis of *N*-(4-chloro-3-[6-nitro-1*H*-imidazo[*4,5-b*]pyridin-2-yl]phenyl)furan-2-carboxamide (8)

A mixture of 5-nitropyridine-2,3-diamine (6 g, 38.93 mmol, 1.00 equiv) and 2-chloro-5-(furan-2-amido)benzoic acid (**7**) (10.4 g, 39.15 mmol, 1.00 equiv) in polyphosphoric acid (PPA) (100 mL) was stirred overnight at 130 °C. The reaction was then poured into water/ice and the pH value of the mixture was adjusted to 9 with sodium carbonate. The solids were collected by filtration and applied onto a silica gel column with ethyl acetate/petroleum ether (3/1) to give 3.9 g (26%) of *N*-(4-chloro-3-[6-nitro-1*H*-imidazo[*4,5-b*]pyridin-2-yl]phenyl)furan-2-carboxamide (**8**) as a light yellow solid. ^{1}H NMR (400 MHz, DMSO) δ 10.50 (s, 1H), 9.19 (d, *J* = 2.6 Hz, 1H), 8.73 (s, 1H), 8.43 (d, *J* = 2.6 Hz, 1H), 8.03 – 7.90 (m, 4H), 7.61 (d, *J* = 8.9 Hz, 1H), 7.41 (d, *J* = 3.6 Hz, 1H), 6.79 – 6.67 (m, 1H). MS *m/z* 383.9 $(M+H)^+$.

3.3.3. Synthesis *N*-(3-[6-amino-1*H*-imidazo[*4,5-b*]pyridin-2-yl]-4-chlorophenyl)furan-2-carboxamide (9)

To a suspension of *N*-(4-chloro-3-[6-nitro-1*H*-imidazo[*4,5-b*]pyridin-2-yl]phenyl)furan-2-carboxamide (3.9 g, 10.16 mmol, 1.00 equiv) in ethanol (50 mL) was added $SnCl_2 \cdot 2H_2O$ (3.4 g, 15.04 mmol, 1.48 equiv) and the resulting mixture was heated to reflux overnight. The reaction mixture was concentrated under vacuum and diluted with H_2O. The pH value of the mixture was adjusted to 9 with saturated sodium carbonate. The solids were collected by filtration and applied onto a silica gel column with ethyl acetate/PE (3/1) to give 1.95 g (54%) of *N*-(3-[6-amino-1*H*-imidazo[*4,5-b*]pyridin-2-yl]-4-chlorophenyl)furan-2-carboxamide (**9**) as a yellow solid. ^{1}H-NMR: (CD_3OD, 400 MHz): 8.16 (d, *J* = 2.4 Hz, 1H), 7.97-8.10 (m, 2H), 7.78 (d, *J* = 0.8 Hz, 1H), 7.65 (d, *J* = 20.0 Hz, 1H), 7.31-7.41 (m, 2H), 6.68 (dd, *J* = 3.6, 2.0 Hz, 1H. MS $(M+H)^+$=354.

3.3.4. Synthesis of Isopropyl (2-(2-chloro-5-(furan-2-carboxamido)phenyl)-1H-imidazo[4,5-b]pyridin-6-yl)carbamate (GNF3943) (10)

To a 20 mL vial was transferred N-(3-(6-amino-1H-imidazo[4,5-b]pyridin-2-yl)-4-chlorophenyl)furan-2-carboxamide **9** (80 mg, 0.225 mmol) in dimethylformamide (4 mL) followed by addition of pyridine (2 drops), and the reaction mixture was stirred at 0 °C for 10 minutes. At this point was added isopropyl carbonochloridate (1 M solution in toluene, 1.45 mmols, 6.4 eq). The reaction mixture was stirred overnight while slowly warming up to room temperature. The presence of desired peak (M+H (440)) was confirmed by LC/MS. The reaction mixture was then quenched with saturated sodium carbonate solution to neutralize the extra acid chloride and to make the solution basic (pH 8-9). The reaction was extracted with ethyl acetate (3x10 mL), and the resulting organics were dried over sodium sulfate, filtered, and dried under vacuum. The resulting residue was purified via ISCO column chromatography using (0-100% ethyl acetate/hexane) to provide 53 mg, 0.119 mmol, 53% of the desired compound. ^{1}H NMR (400 MHz, MeOD) δ 8.28 (d, *J* = 22.1, 2H), 8.10 (s, 1H), 7.88 (s, 1H), 7.67 (d, *J* = 1.0, 1H), 7.51 (d, *J* = 8.8, 1H), 7.24 – 7.16 (m, 1H), 6.56 (dd, *J* = 1.7, 3.5, 1H), 4.91 (dt, *J* = 6.2, 12.5, 1H), 1.24 (d, *J* = 6.2, 6H). M/Z=440.1(M+1)

3.4. Synthesis of GNF8000; isopropyl (2-(2-fluoro-5-(furan-2-carboxamido)phenyl) imidazo[1,2-a]pyrimidin-6-yl)carbamate

3.4.1. Synthesis of 1-(2-fluoro-5-nitrophenyl)ethan-1-one (11)

A 3,000 mL three necked flask equipped with a mechanic stirrer was charged with concentrated H_2SO_4 (720 mL) and cooled to -40 °C. 1-(2-fluorophenyl)ethanone (180 g, 1.3 mol) was added, followed by addition of a mixture of fuming HNO_3 (106.2 mL) in concentrated H_2SO_4 (260 mL) dropwise over 45 minutes. This mixture was stirred at this temperature for 15 minutes, poured into ice (8 kg), and extracted with ethyl acetate (2000 mL x 2). The combined ethyl acetate layer was washed with saturated $NaHCO_3$ solution (800 mL x 3), brine (800 mL), dried with anhydrous sodium sulfate, and concentrated under vacuum. The residue was crystallized with petroleum ether to give compound **11** (200 g, yield: 84%) as a

yellow solid. ^{1}H NMR (400 MHz, $CDCl_3$) δ 7.34 (t, *J* = 9.29 Hz, 1H), 8.33-8.48 (m, 1H), 8.78 (dd, *J* = 6.15, 2.89 Hz, 1H).

3.4.2. Synthesis of 2-bromo-1-(2-fluoro-5-nitrophenyl)ethan-1-one (12)

To a solution of compound **11** (126 g, 0.688 mol) in acetic acid (860 mL) and 40% HBr solution (825.6 mL) at 0 °C, was added a solution of Br_2 (110 g, 0.688 mol) in acetic acid (344 mL) in one portion. This mixture was stirred at room temperature overnight, diluted with water (3000 mL), and extracted with 50% ethyl acetate/petroleum ether (1500 mL x 2). The combined organic layer was washed with a saturated $NaHCO_3$ solution (1000 mL x 2), brine (1000 mL), dried with anhydrous sodium sulfate and concentrated. The residue was purified by column chromatography on silica gel (20% EA/PE) to give the compound **12** (150 g, yield: 83%) as a white solid.^{1}H NMR (400 MHz, $CDCl_3$) δ 8.85 (dd, *J* = 5.90, 2.89 Hz, 1H), 8.42-8.58 (m, 1H), 7.42 (t, *J* = 9.29 Hz, 1H), 4.52 (d, *J* = 2.01 Hz, 2H).

3.4.3. Synthesis of Isopropyl (2-aminopyrimidin-5-yl)carbamate (13)

A suspension of 5-nitropyrimidine-2-amine (1 eq.) and Pd/C (0.05 eq.) in ethanol (0.1 mM) was stirred under hydrogen atmosphere overnight at room temperature to give of 2,5-diaminopyrimidine. The mixture was then filtered and concentrated under vacuum. The residue (1 eq.) was subjected to coupling with isopropylcarbonochloridate (1.5 eq.) in anhydrous pyridine (0.3 mM) overnight at room temperature. The mixture was concentrated under vacuum, and the residue was extracted with ethyl acetate, washed with brine, dried over anhydrous MgSO4 (s), filtered and concentrated under vacuum to give **13** as a yellow solid. m/z (ESI): 196 ($M + H^+$).

3.4.4. Synthesis of isopropyl (2-(2-fluoro-5-nitrophenyl)imidazo[1,2-a]pyrimidin-6-yl)carbamate (14)

Into a 500 mL round-bottom flask, was placed 2-bromo-1-(2-fluoro-5-nitrophenyl)ethan-1-one **12** (30 g, 114.49 mmol, 1 eq.), propan-2-yl N-(2-aminopyrimidin-5-yl)carbamate (11.2 g, 57.08 mmol, 0.5 eq.) and

acetone (200 mL). The resulting solution was stirred overnight at 70 °C. The reaction mixture was cooled down and the solids were collected by filtration resulting in 15 g (36%) of propan-2-yl N-[2-(2-fluoro-5-nitrophenyl)imidazo[1,2-a]pyrimidin-6-yl]carbamate (**14**) as a brown solid.

3.4.5. Synthesis of isopropyl (2-(5-amino-2-fluorophenyl)imidazo[1,2-a]pyrimidin-6-yl)carbamate (15)

Into a 1 L round-bottom flask was placed tetrahydrofuran (500 mL), Raney Ni (15 g) and propan-2-yl N-[2-(2-fluoro-5-nitrophenyl)imidazo[1,2-a]pyrimidin-6-yl]carbamate **14** (8 g, 22.26 mmol, 1 eq.). The resulting solution was stirred overnight at room temperature under an atmosphere of hydrogen. The solids were filtered out, and washed with methanol (200 mL x 4). The resulting mixture was concentrated under vacuum to give 7 g (95%) of propan-2-yl N-[2-(5-amino-2-fluorophenyl)imidazo[1,2-a]pyrimidin-6-yl]carbamate (**I5**) as a brown solid. ^{1}H NMR (400 MHz, DMSO-d_6) δ 9.94 (s, 1H), 9.24 (s, 1H), 8.46-8.47 (m, 1H), 8.26-8.28 (m, 1H), 7.51-7.53 (m, 1H), 6.96-7.02 (m, 1H), 6.55-6.59 (m, 1H), 4.89-4.98 (m, 1H), 3.17 (s, 2H), 1.07-1.30(m, 6H). MS *m/z*= 330 (M+1).

3.4.6. Synthesis of isopropyl (2-(2-fluoro-5-(furan-2-carboxamido)phenyl) imidazo[1,2-a]pyrimidin-6-yl)carbamate (GNF8000) (16)

In a 40 mL vial, pyridine (10 mL) was added to intermediate **15** (0.5 g, 1.518 mmol) to give a yellow solution. To this solution was added furan-2-carbonyl chloride (0.198 g, 1.518 mmol) at 0 °C and the resulting mixture was stirred for 1 hour. The reaction mixture was quenched with 60 mL of water and extracted with ethyl acetate. The same step was repeated once more time to remove any extra pyridine. All organic phases were combined, dried over sodium sulfate and purified by flash chromatography to give product **16** (ethyl acetate/methanol= 0-10%). ^{1}H NMR (400 MHz, DMSO-d_6) δ 10.43 (s, 1H), 10.06 (s, 1H), 9.36 (s, 1H), 8.69 (dd, *J* = 2.8, 6.9 Hz, 1H), 8.56 (d, *J* = 2.7 Hz, 1H), 8.45 (d, *J* = 4.2 Hz, 1H), 8.02 (d, *J* = 1.0 Hz, 1H), 7.95-7.85 (m, 1H), 7.46 (d, *J* = 3.4 Hz, 1H), 7.37 (dd, *J* = 9.0, 10.9 Hz, 1H),

6.78 (dd, *J* = 1.7, 3.5 Hz, 1H), 5.00 (dt, *J* = 6.3, 12.5 Hz, 1H), 1.35 (d, *J* = 6.2 Hz, 6H). MS *m/z* = 424 (M+1).

3.5. Synthesis of GNF3849; N-(4-fluoro-3-(6-phenyl-[1,2,4]triazolo[1,5-a]pyrimidin-2-yl)phenyl)-2,4-dimethyloxazole-5-carboxamide

3.5.1. Synthesis of 2-(2-fluoro-5-nitrophenyl)-6-phenyl-[1,2,4]triazolo[1,5-a]pyrimidine (17)

To a solution of compound **3** (0.5 g, 2.24 mmol) in AcOH (5 mL) was added 2-phenylmalonaldehyde (0.39 g, 2.7 mmol). The mixture was then heated to 100 °C and stirred for 4 hours. The mixture was allowed to cool to room temperature, water (10 mL) was added, the solids filtered, and the filter cake was washed with tetrahydrofuran, and dried under vacuum to give compound **17** (0.36 g, 48% yield). ^{1}H NMR (400 MHz, DMSO) 9.93 (d, *J* = 2.4, 1H), 9.38 (d, *J* = 2.8, 1H), 8.90 (s, 1H), 7.93 (d, *J* = 7.78, 2H), 7.69 (d, *J* = 8.53, 1H), 7.61-7.50 (m, 2H), 7.31 (t, *J* = 7.40, 1H), 6.88 (s, 1H).

3.5.2. Synthesis of 4-fluoro-3-(6-phenyl-[1,2,4]triazolo[1,5-a]pyrimidin-2-yl)aniline (18)

To a solution of compound **17** (2.5 g, 7.4 mmol) in tetrahydrofuran (200 mL) was added ZnI_2 (1.2 g, 3.7 mmol) and Raney Nickel (3.5 g). This mixture was stirred at room temperature for 4 hour under H_2 at 50 psi, then the mixture was filtrated and washed with methanol (20 mL) to give compound **18** (2.0 g, 87% yield). ^{1}H NMR (400 MHz, DMSO) 9.81 (d, *J* = 2.4, 1H), 9.27 (d, *J* = 2.8, 1H, 7.90 (d, *J* = 7.6, 2H), 7.58-7.53 (m, 2H), 7.45-7.50 (m, 2H), 7.09-7.05 (m, 1H), 6.74-6.70 (m, 1H), 5.22 (s, 2H). M/Z 306.1 ($M+H^+$).

3.5.3. Synthesis of N-(4-fluoro-3-(6-phenyl-[1,2,4]triazolo[1,5-a]pyrimidin-2-yl)phenyl)-2,4-dimethyloxazole-5-carboxamide (GNF3849) (19)

To a solution of 2,4-dimethyloxazole-5-carboxylic acid (0.56 g, 3.9 mmol) in dimethylformamide (30 mL) was added DIEA (0.85 g, 6.66 mmol) and HATU (1.5 g, 3.9 mmol). This mixture was stirred at room temperature for 30 minutes, then compound **18** (1.0 g, 3.28 mmol) was added. The mixture was then

stirred at room temperature for 4 hours, diluted with water (50 mL) and extracted with tetrahydrofuran/ ethyl acetate (100 mL /50 mL), the organic layer was dried over sodium sulfate and concentrated to give the crude product. It was purified by HPLC to give product **19** (0.91 g, yield, 65%) as a white solid. ^{1}H NMR (400 MHz, MeOD) 9.49 (d, *J* = 2.4, 1H), 9.22 (d, *J* = 2.4, 1H), 8.51 (dd, *J* = 6.4, 2.8, 1H), 7.90 (ddd, *J* = 8.9, 4.2, 2.8, 1H), 7.86-7.76 (m, 2H), 7.63-7.55 (m, 2H), 7.54-7.45 (m, 1H), 7.32 (dd, *J* = 10.4, 9.0, 1H), 2.56 (s, 3H), 2.47 (s, 3H). M/Z= 429.2 ($M+H^+$).

3.6. Synthesis of GNF2636; isopropyl (2-(2-chloro-5-(furan-2-carboxamido)phenyl)imidazo[1,2-a]pyrimidin-6-yl)carbamate

3.6.1. Synthesis of isopropyl (2-(2-chloro-5-nitrophenyl)imidazo[1,2-a]pyrimidin-6-yl)carbamate (20)

Into a 500-mL round-bottom flask, was placed **13** (1.75 g, 6.3 mmol, 1.2 equiv), acetone (400 mL) and 2-bromo-1-(2-chloro-5-nitrophenyl)ethan-1-one (1.0 g, 5.3 mmol). The resulting solution was stirred overnight at 70 °C. The reaction mixture was cooled, the solvent evaporated, the resulting material suspended in methanol, and then solids collected by filtration resulting in product **20** (0.75 g, 38% yield). 1H NMR (400 MHz, DMSO-D6) δ 10.08 (s, 1H), 9.34 (s, 1H), 9.08 (s, 1H), 8.86 (s, 1H), 8.56 (s, 1H), 8.19 (d, J = 8.7, 1H), 7.88 (d, J = 8.8, 1H), 4.95 (m, 1H), 1.30 (m, 6H). MS m/z (ESI) = 377 (M +).

3.6.2. Synthesis of isopropyl (2-(5-amino-2-chlorophenyl)imidazo[1,2-a]pyrimidin-6-yl)carbamate (21)

In a round-bottom flask, **20** (300 mg, 0.77 mmol) was taken up in methanol (20 mL) and SnCl2 (3 equivalents) was added. The resulting mixture was stirred for 2 hours at reflux. The reaction mixture was concentrated under vacuum and the crude material was purified by flash column chromatography (hexane/ ethyl acetate solvent system followed by DCM/methanol solvent system) resulting in **21** (265 mg, 96%) as a yellow solid. 1H-NMR: (300 MHz, MeOD): 9.30 (s, 1H), 8.51 (d, J = 2.1 Hz, 1H), 8.37 (s,

1H), 7.37 (d, J = 1.8 Hz, 1H), 7.23 (d, J = 6.6 Hz, 1H), 6.72-6.74 (m, 1H), 5.01-5.07 (m, 1H), 1.24-1.36 (m, 6H). MS m/z = 346 (M+H+).

3.6.3. Synthesis of isopropyl (2-(2-chloro-5-(furan-2-carboxamido)phenyl)imidazo[1,2-a] pyrimidine-6-yl)carbamate (GNF2636) (22)

To a suspension of compound **21** (20 mg, 0.06 mmol) in pyridine (2 mL) in a vial was added 2-furoyl chloride (1.5 equivalents) at room temperature. After stirring overnight, the reaction was concentrated and the resulting residue was purified by prep HPLC to afford the product **22** (5 mg, 19% yield). 1H NMR (400 MHz, methanol-*d*4) δ9.57 (s, 1H), 8.76 (d, *J* = 2.6 Hz, 1H), 8.52 (s, 1H), 8.31 (d, *J* = 2.6 Hz, 1H), 7.89 – 7.69 (m, 2H), 7.62 (d, *J* = 8.8 Hz, 1H), 7.32 (d, *J* = 3.5 Hz, 1H), 6.68 (dd, *J* = 3.5, 1.7 Hz, 1H), 5.14 – 4.97 (m, 1H), 1.35 (d, *J* = 6.3 Hz, 6H). MS *m/z* = 440.2 (M+H).

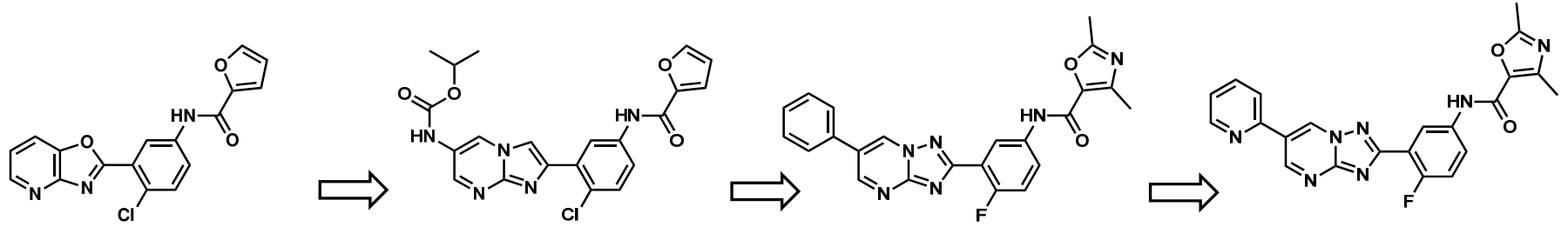

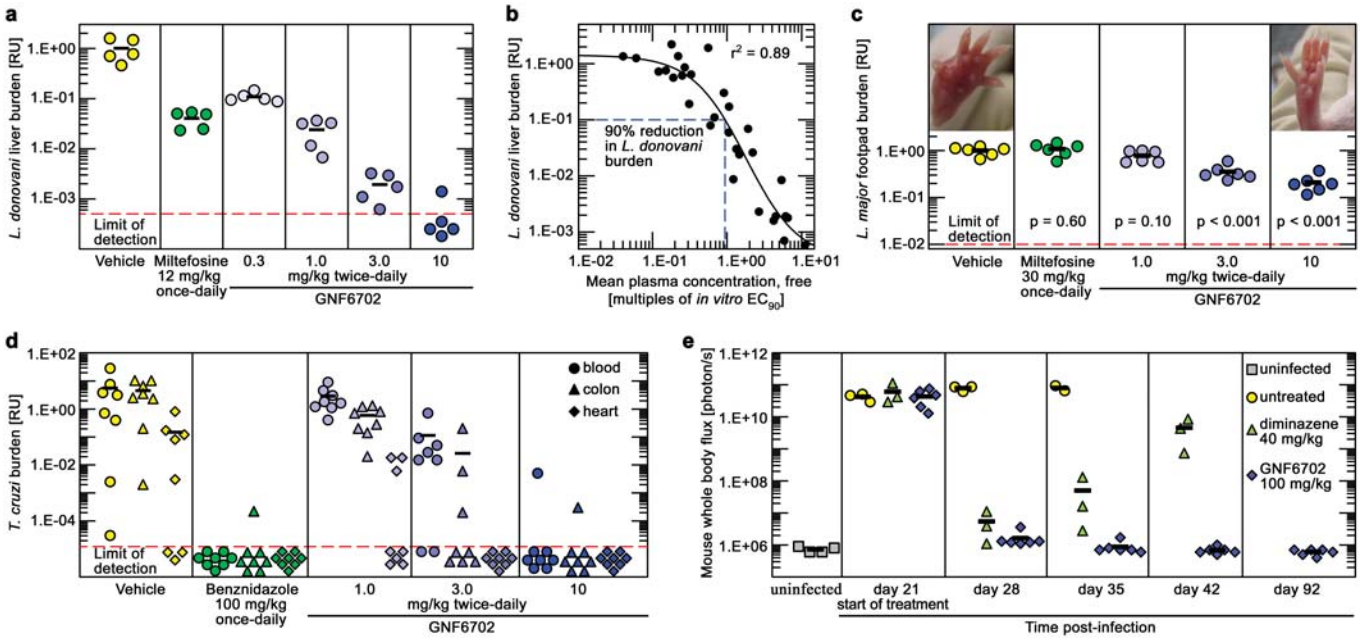
a
L. donovani liver burden [RU]
1.E+00
1.E-01
1.E-02
1.E-03
Limit of detection
Vehicle
Miltefosine 12 mg/kg once-daily
0.3
1.0
3.0
10
mg/kg twice-daily
GNF6702
b
L. donovani liver burden [RU]
r2 = 0.89
90% reduction in L. donovani burden
1.E-02
1.E-01
1.E+00
1.E+01
Mean plasma concentration, free [multiples of in vitro EC90]
c
L. major footpad burden [RU]
1.E+00
1.E-01
1.E-02
Limit of detection
p = 0.60
p = 0.10
p < 0.001
p < 0.001
Vehicle
Miltefosine 30 mg/kg once-daily
1.0
3.0
10
mg/kg twice-daily
GNF6702
d
T. cruzi burden [RU]
1.E+02
1.E+00
1.E-02
1.E-04
blood
colon
heart
Limit of detection
Vehicle
Benznidazole 100 mg/kg once-daily
1.0
3.0
10
mg/kg twice-daily
GNF6702
e
Mouse whole body flux [photon/s]
1.E+12
1.E+10
1.E+08
1.E+06
uninfected
untreated
diminazene 40 mg/kg
GNF6702 100 mg/kg
uninfected
day 21
start of treatment
day 28
day 35
day 42
day 92
Time post-infection

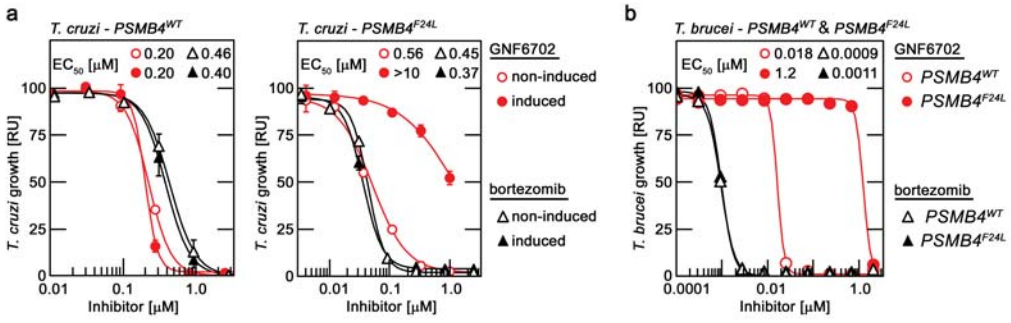
a
T. cruzi - PSMB4WT
EC50 [µM]
0.20 Δ0.46
0.20 ▲0.40
T. cruzi - PSMB4F24L
EC50 [µM]
0.56 Δ0.45
>10 ▲0.37
GNF6702
non-induced
induced
bortezomib
Δ non-induced
▲ induced
T. cruzi growth [RU]
Inhibitor [µM]
b
T. brucei - PSMB4WT & PSMB4F24L
EC50 [µM]
0.018 Δ0.0009
1.2 ▲0.0011
GNF6702
PSMB4WT
PSMB4F24L
bortezomib
Δ PSMB4WT
▲ PSMB4F24L
T. brucei growth [RU]
Inhibitor [µM]

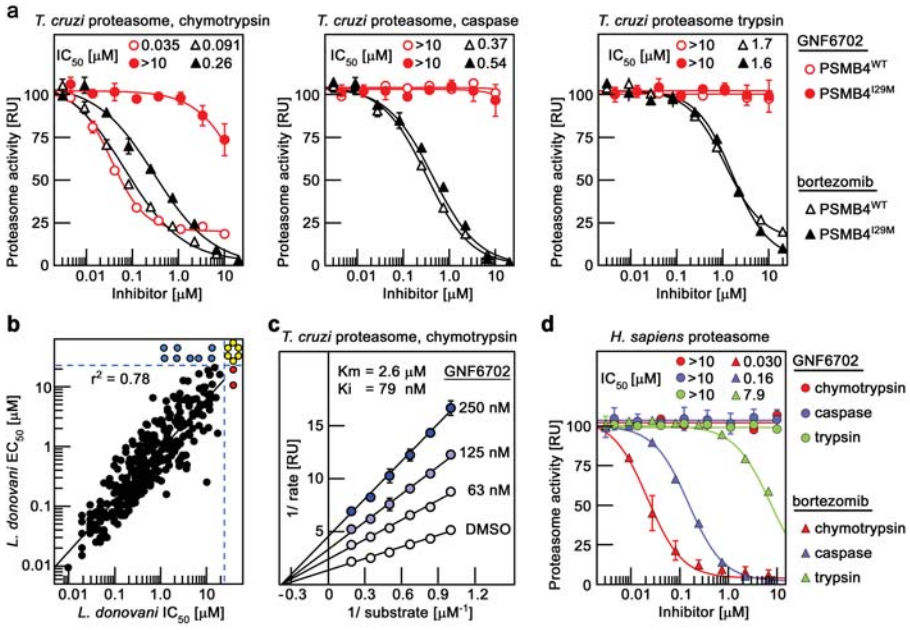
a
T. cruzi proteasome, chymotrypsin
IC50 [μM]
0.035
0.091
>10
0.26
Proteasome activity [RU]
Inhibitor [μM]
T. cruzi proteasome, caspase
IC50 [μM]
>10
0.37
>10
0.54
T. cruzi proteasome trypsin
IC50 [μM]
>10
1.7
>10
1.6
GNF6702
PSMB4WT
PSMB4I29M
bortezomib
PSMB4WT
PSMB4I29M
b
r2 = 0.78
L. donovani EC50 [μM]
L. donovani IC50 [μM]
c
T. cruzi proteasome, chymotrypsin
Km = 2.6 μM
Ki = 79 nM
GNF6702
250 nM
125 nM
63 nM
DMSO
1/ rate [RU]
1/ substrate [μM-1]
d
H. sapiens proteasome
IC50 [μM]
>10
0.030
>10
0.16
>10
7.9
GNF6702
chymotrypsin
caspase
trypsin
bortezomib
chymotrypsin
caspase
trypsin
Proteasome activity [RU]
Inhibitor [μM]

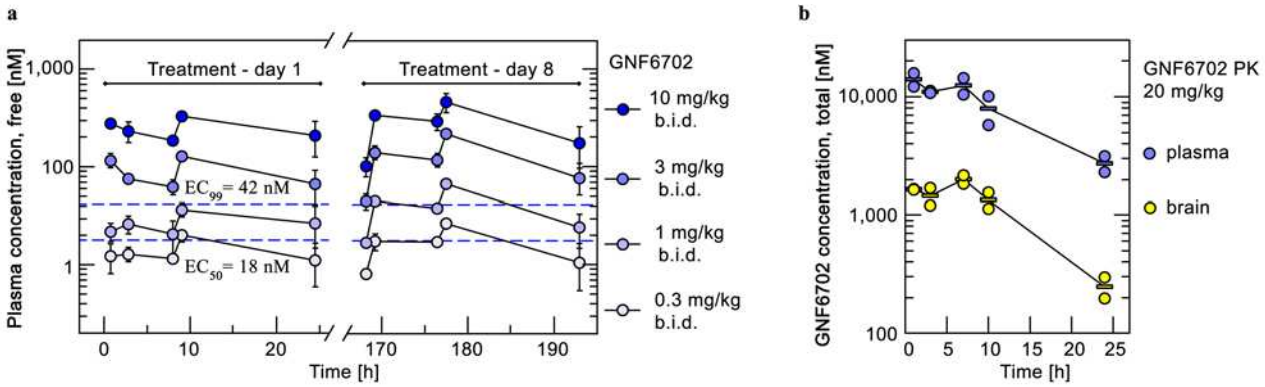
a
Plasma concentration, free [nM]
1,000
100
1
Treatment - day 1
Treatment - day 8
EC99 = 42 nM
EC50 = 18 nM
0
10
20
170
180
190
Time [h]
GNF6702
10 mg/kg b.i.d.
3 mg/kg b.i.d.
1 mg/kg b.i.d.
0.3 mg/kg b.i.d.
b
GNF6702 concentration, total [nM]
10,000
1,000
100
0
5
10
15
20
25
Time [h]
GNF6702 PK
20 mg/kg
plasma
brain

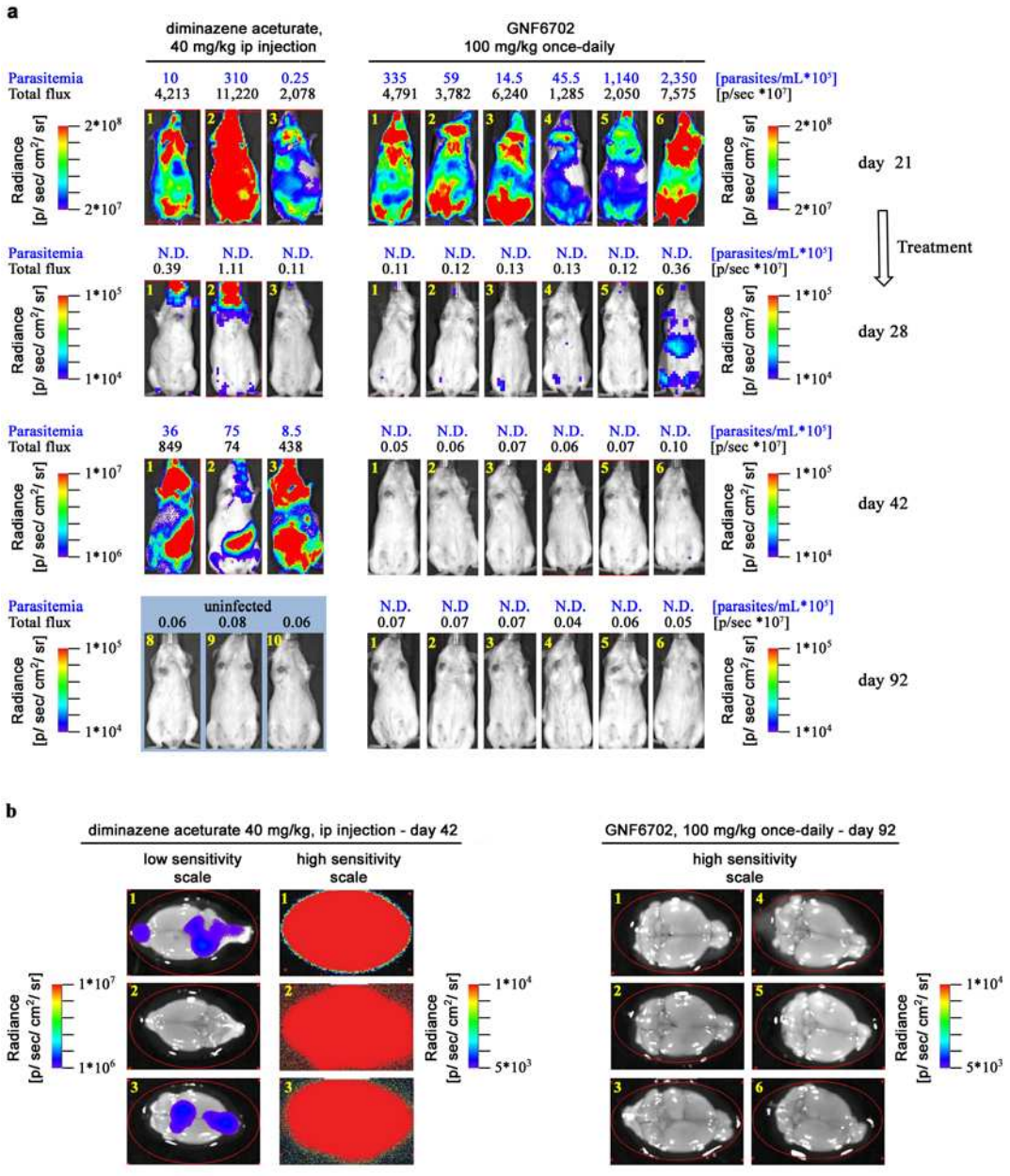
a
diminazene aceturate, 40 mg/kg ip injection
GNF6702 100 mg/kg once-daily
Parasitemia
Total flux
10 310 0.25
4,213 11,220 2,078
335 59 14.5 45.5 1,140 2,350
4,791 3,782 6,240 1,285 2,050 7,575
[parasites/mL*10^5]
[p/sec *10^7]
Radiance [p/ sec/ cm^2/ sr]
2*10^8
2*10^7
day 21
Treatment
N.D. N.D. N.D.
0.39 1.11 0.11
N.D. N.D. N.D. N.D. N.D. N.D.
0.11 0.12 0.13 0.13 0.12 0.36
1*10^5
1*10^4
day 28
36 75 8.5
849 74 438
N.D. N.D. N.D. N.D. N.D. N.D.
0.05 0.06 0.07 0.06 0.07 0.10
1*10^7
1*10^6
day 42
uninfected
0.06 0.08 0.06
N.D. N.D N.D. N.D. N.D. N.D.
0.07 0.07 0.07 0.04 0.06 0.05
day 92
b
diminazene aceturate 40 mg/kg, ip injection - day 42
low sensitivity scale
high sensitivity scale
GNF6702, 100 mg/kg once-daily - day 92
high sensitivity scale
1*10^7
1*10^6
1*10^4
5*10^3

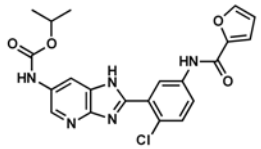

GNF3943

L. donovani EC_{50} = 380 ± 23 nM
T. brucei EC_{50} = 33 ± 9.4 nM
T. cruzi EC_{50} = 120 ± 12 nM
3T3 CC_{50} = 4.5 ± 0.9 μM
Macrophage CC_{50} = 9.8 ± 2.4 μM
F = 75 %
CL = 17.7 $mL*min^{-1}*kg^{-1}$

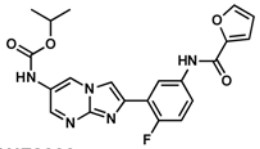

GNF8000

L. donovani EC_{50} = 320 ± 7.1 nM
T. brucei EC_{50} = 73 ± 2.9 nM
T. cruzi EC_{50} = 154 ± 12 nM
3T3 CC_{50} > 20 μM
Macrophage CC_{50} = 18 ± 2.1 μM
F = 10 %
CL = 8.8 $mL*min^{-1}*kg^{-1}$

a

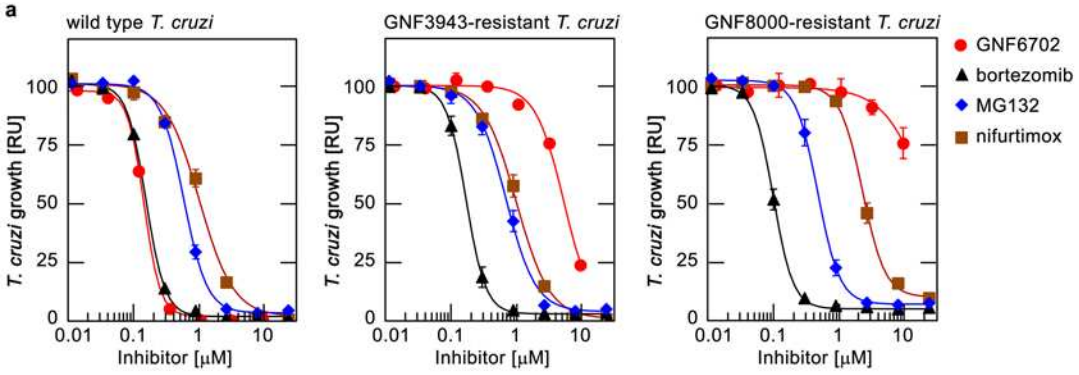

b

	wt *T. cruzi*	GNF3943^{R} *T. cruzi*	GNF8000^{R} *T. cruzi*
GNF6702 EC_{50} [μM]	0.15 ± 0.002	5.5 ± 0.016	> 10
bortezomib EC_{50} [μM]	0.16 ± 0.006	0.12 ± 0.020	0.10 ± 0.007
MG132 EC_{50} [μM]	0.61 ± 0.015	0.76 ± 0.071	0.48 ± 0.052
nifurtimox EC_{50} [μM]	1.0 ± 0.09	1.0 ± 0.11	2.4 ± 0.15

c

	T. cruzi ectopic PSMB4^{WT}		*T. cruzi* ectopic PSMB4^{F24L}		*T. brucei* ectopic PSMB4^{WT}	*T. brucei* ectopic PSMB4^{F24L}
	non-induced	induced	non-induced	induced	constitutive	constitutive
GNF6702 [μM]	0.20 ± 0.007	0.20 ± 0.023	0.56 ± 0.029	> 10	0.018 ± 0.0018	1.2 ± 0.013
bortezomib [μM]	0.46 ± 0.059	0.40 ± 0.057	0.45 ± 0.008	0.37 ± 0.015	0.00094 ± 0.00005	0.0011 ± 0.00026

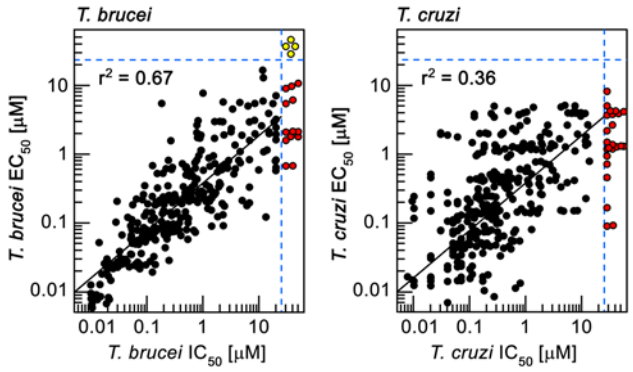
T. brucei
r² = 0.67
T. brucei EC50 [μM]
T. brucei IC50 [μM]
0.01
0.1
1
10
T. cruzi
r² = 0.36
T. cruzi EC50 [μM]
T. cruzi IC50 [μM]

a

```
                                                  L   M
L. donovani     1 MAETAIAFRCQDYVMVAAAGLNAFYYIKITDAEDKITQLDTHQLIACTGE
T. cruzi        1 MSETTIAFRCNSFVLVAAAGLNAFYYIKIMDTEDKVTQLDSHKVVACAGE
T. brucei       1 MAETTIGFRCQDFVLVAAAGLNAFYYIKITDTEDKITELDSHKVVACAGE
H.sapiens       1   MEYLIGIQGPDYVLVASDRVAASNIVQMKDDHDKMFKMSEKILLLCVGE

L. donovani    51 NGPRVNFTEYIKCNLMLNRMRQHGRHSSCDSTANFMRNCLASAIRSREGA
T. cruzi       51 NGPRVNFVEYIKCNMALKRMREHGRVIRTSAAASFMRNALAGALRSRDGA
T. brucei      51 NGPRTHFVEYVKCNMALKKMREHGRMISTHATASFMRNTLAGALRSRDGL
H.sapiens      50 AGDTVQFAEYIQKNVQLYKMR-NGYELSPTAAANFTRRNLADCLRSRT-P

L. donovani   101 YQVNCLFAGYDMPVSEDDDGAVGPQLFYLDYLGTLQAVPYGCHGYGACFV
T. cruzi      101 YLVNCLLAGYDVAASSDDDIATGPHLYYMDYLGTMQEVPYGCHGYGASFV
T. brucei     101 YPVNCLLAGFDVPASAEDDVATGAHLYYLDYLGTMQEVPYGCHGYGAPFV
H.sapiens      98 YHVNLLLAGYDE-------HEGPALYYMDYLAALAKAPFAAHGYGAFLT

L. donovani   151 TALLDCLWRPDLTQQEGLELMQKCCDEVKRRVVISNSYFFVKAVTKNGVE
T. cruzi      151 IAMLDRLWRPDLTAQEAVDLMQKCCDEVKKRVVISNDKFICKAVTENGVE
T. brucei     151 TAMLDRMWRPNLTAQEGVDLMQKCCDEVKKRVVVSNNTFICKAVTKDGVE
H.sapiens     140 LSILDRYYTPTISRERAVELLRKCLEELQKRFILNLPTFSVRIIDKNGIH

L. donovani   201 VITAVH
T. cruzi      201 LVNTVS
T. brucei     201 LVNTVS
H.sapiens     190 DLDNISFPKQGS
```

b

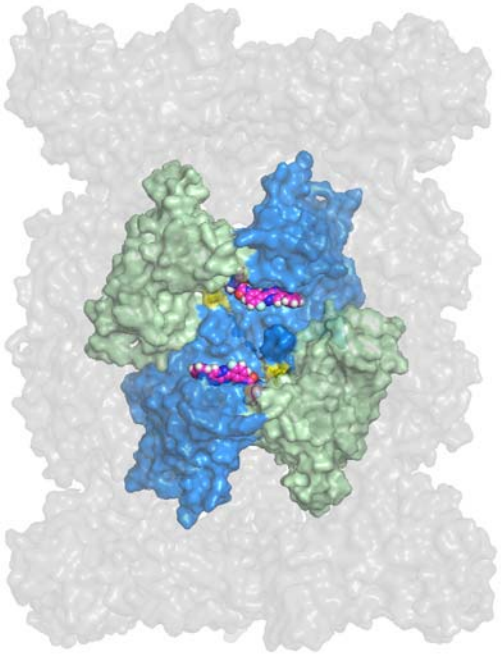

c

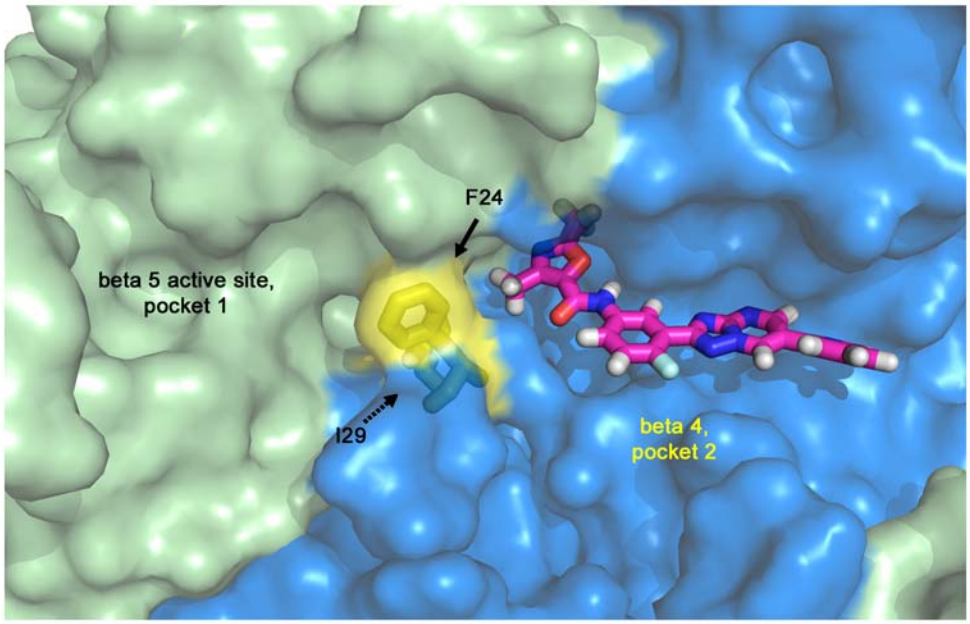

a

T. cruzi epimastigotes

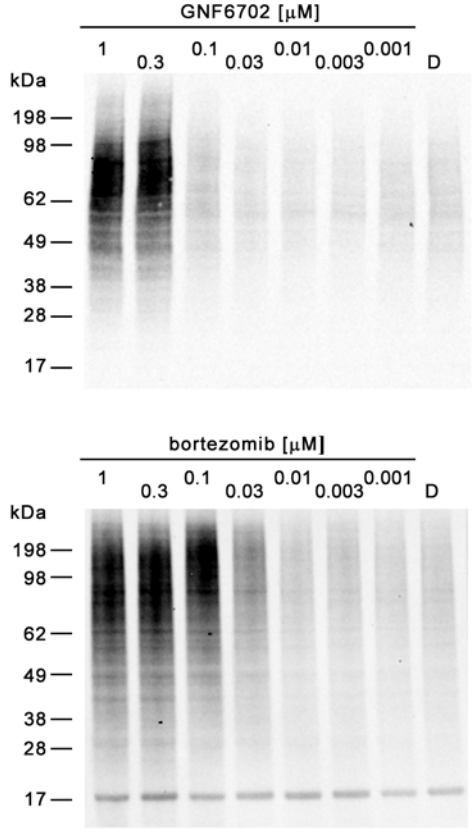

b

3T3 cells

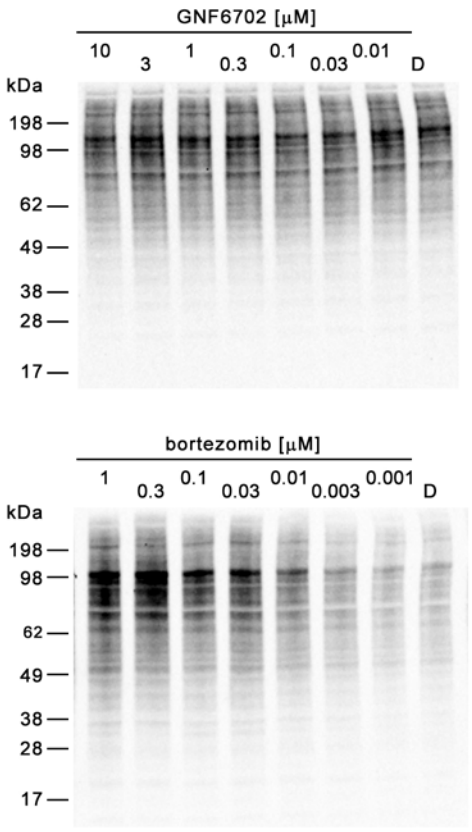

c

	T. cruzi	3T3
GNF6702 EC_{50} [μM]	0.13 ± 0.010	> 10
bortezomib EC_{50} [μM]	0.062 ± 0.001	0.040 ± 0.008

Supplementary Figure 1

a Western blots of three sets of cell lysates from GNF6702-treated *T. cruzi* epimastigotes

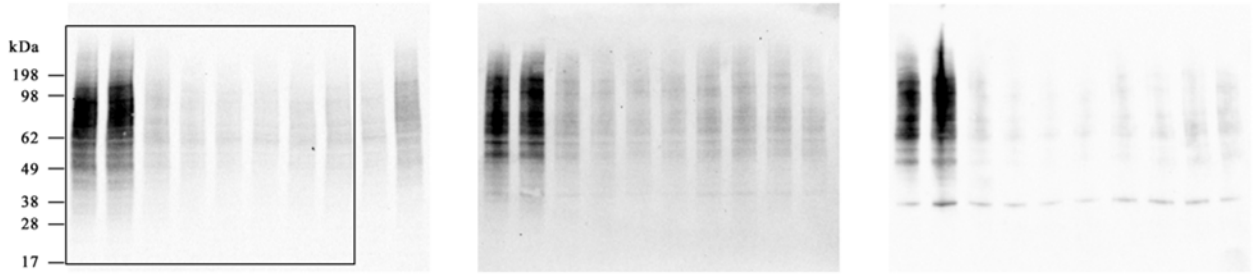

Extended Data Fig. 7a, upper panel

b Western blots of three sets of cell lysates from bortezomib-treated *T. cruzi* epimastigotes

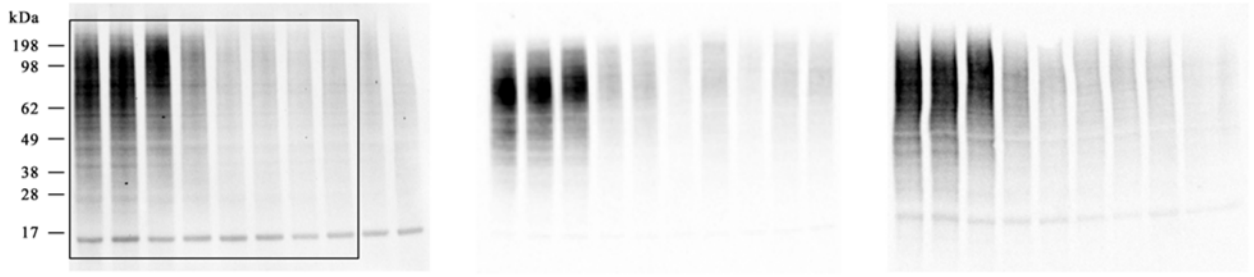

Extended Data Fig. 7a, lower panel

c Western blots of three sets of cell lysates from GNF6702-treated 3T3 cells

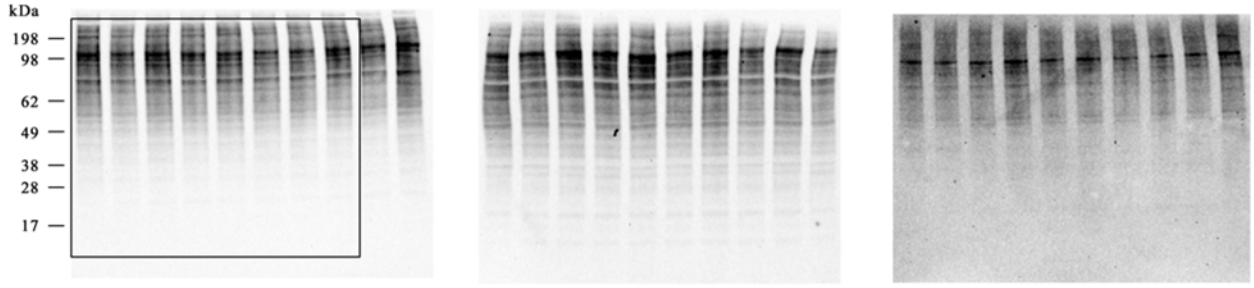

Extended Data Fig. 7b, upper panel

d Western blots of three sets of cell lysates from bortezomib-treated 3T3 cells

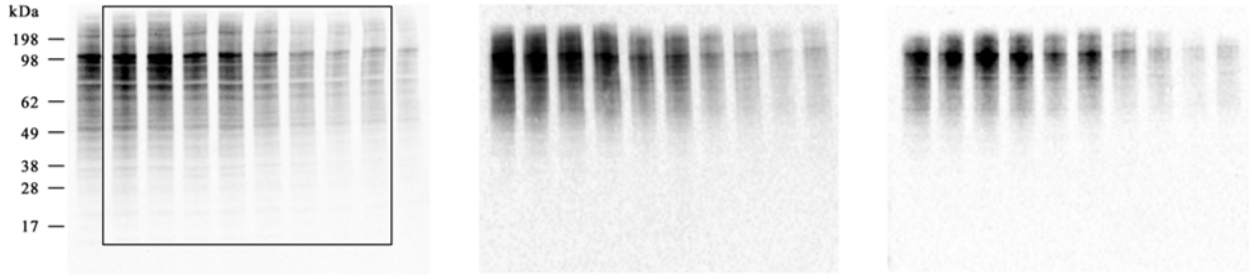

Extended Data Fig. 7b, lower panel

Excel files

1. Supplementary Table 1

   Small molecule screening data from *Leishmania donovani* axenic amastigote growth inhibition HTS.

2. Supplementary Table 2

   Small molecule screening data from *Trypanosoma brucei* bloodstream form trypomastigote growth inhibition HTS.

3. Supplementary Table 3

   Small molecule screening data from *Trypanosoma cruzi* intracellular trypomastigote growth inhibition HTS.

4. Supplementary Table 4

   Time course of parasitemia in mice infected with bioluminescent *T. brucei* during and after treatment with diminazene aceturate and GNF6702

5. Supplementary Table 5

   Time course of whole body bioluminescence in mice infected with bioluminescent *T. brucei* during and after treatment with diminazene aceturate and GNF6702

6. Supplementary Table 6

   Trypanosoma brucei bioluminescence of *ex vivo* brains obtained from parasite-infected mice after treatment with diminazene aceturate and GNF6702.

7. Supplementary Table 7

   20S proteasome subunits identified in purified *T. cruzi* proteasome.

8. Supplementary Table 8

   Amino acid sequences of predicted *Trypanosoma cruzi* 20S proteasome alpha and beta subunits.

9. Supplementary Table 9

   GNF6702 profile in a panel of mammalian receptors, enzymes and ion channels.

10. Supplementary Table 10

    GNF6702 inhibition profile in a cell-based Ba/F3 panel of Tel-activated human tyrosine kinases.

11. Supplementary Table 11

    GNF6702 ADME profile.